

Intelligent Reflecting Surface Enhanced Indoor Robot Path Planning: A Radio Map based Approach

Xidong Mu, *Student Member, IEEE*, Yuanwei Liu, *Senior Member, IEEE*,
Li Guo, *Member, IEEE*, Jiaru Lin, *Member, IEEE*, and
Robert Schober, *Fellow, IEEE*

Abstract

Integrating robots into cellular networks creating connected robotic users has emerged as a promising technology for future smart cities and smart factories due to their low cost and high maneuverability. However, the requirement of establishing stable and high-quality communication links to the robotic users greatly restricts their applicability, especially in indoor environments where obstacles may block the wireless link. To tackle this challenge, in this paper, an indoor robot navigation system is investigated, where an intelligent reflecting surface (IRS) is employed to enhance the connectivity between the access point (AP) and robotic users. Both single-user and multiple-user scenarios are considered. In the single-user scenario, one mobile robotic user (MRU) communicates with the AP. In the multiple-user scenario, the AP serves one MRU and one static robotic user (SRU) employing either non-orthogonal multiple access (NOMA) or orthogonal multiple access (OMA) transmission. The considered system is optimized for minimization of the travelling time/distance of the MRU from a given starting point to a predefined final location, while satisfying constraints on the communication quality of the robotic users. To this end, a *radio map* based approach is proposed to exploit location-dependent channel propagation knowledge. For the single-user scenario, a *channel power gain map* is constructed, which characterizes the spatial distribution of the maximum expected effective channel power gain of the MRU for the optimal IRS phase shifts. Based on the obtained channel power gain map, the communication-aware robot path planning problem is solved by exploiting graph theory. For the multiple-user scenario, a *communication*

Part of this work has been submitted to the IEEE International Conference on Communications (ICC), Montreal, Canada, June 14-18, 2021. [1]

X. Mu, L. Guo, and J. Lin are with the School of Artificial Intelligence and the Key Laboratory of Universal Wireless Communications, Ministry of Education, Beijing University of Posts and Telecommunications, Beijing, China. (email:{muxidong, guoli, jrlin}@bupt.edu.cn).

Y. Liu is with the School of Electronic Engineering and Computer Science, Queen Mary University of London, London, UK. (email:yuanwei.liu@qmul.ac.uk).

R. Schober is with the Institute for Digital Communications, Friedrich-Alexander-University Erlangen-Nürnberg (FAU), Germany (e-mail: robert.schober@fau.de).

rate map is constructed, which characterizes the spatial distribution of the maximum expected rate of the MRU for the optimal power allocation at the AP and the optimal IRS phase shifts subject to a minimum rate requirement for the SRU. The joint optimization problem is efficiently solved by invoking bisection search and successive convex approximation methods. Then, a graph theory based solution for the robot path planning problem is derived by exploiting the obtained communication rate map. Our numerical results show that: 1) the required travelling distance of the MRU can be significantly reduced by deploying an IRS; 2) NOMA yields a higher communication rate for the MRU than OMA; 3) the IRS performance gain is significantly more pronounced for NOMA than for OMA.

I. INTRODUCTION

In the past few decades, robot technology has developed rapidly and has had a significant impact on human life [2]. Specifically, robots can help humans perform repetitive or dangerous tasks, thus liberating human resources and reducing health risks. There is a wide range of robot applications, including cargo/packet delivery, search and rescue, public safety surveillance, environmental monitoring, and automatic industrial production [3, 4]. In terms of their modes of operation, current robots can be loosely classified into two categories, namely, automated robots and connected robots [5]. Based on the equipped sensors and computational resources, automated robots are able to make decisions on their own during a mission. However, they are exceedingly complex due to the large memory, large computational resources, and large number of artificial intelligence based algorithms needed for carrying out sophisticated tasks. In contrast, connected robots accomplish missions relying on information exchange with operators [5]. For instance, a connected robot sends the sensed data (e.g., pictures or videos) to its operator in a real-time manner, and the operator provides further instructions to the connected robot based on the data. Therefore, connected robots are more cost-efficient and less computation-constrained. With the rapid development of fifth-generation (5G) and beyond (B5G) cellular networks, one promising solution is to integrate connected robots into cellular networks as robotic users to be served by base stations (BSs) or access points (APs). Given the ultra-high speed, low latency, and high reliability of 5G/B5G networks, connected robots are expected to become a key technology in the future.

Despite the appealing advantages of connected robots, one crucial limitation is that the communication link may be severely blocked by buildings, trees or other tall objects. The resulting signal *dead zones* can significantly restrict the area of operation and reduce the efficiency of connected robots. Fortunately, with the recent advances in meta-materials, intelligent reflecting surfaces

(IRSs) [6], also known as reconfigurable intelligent surfaces (RISs) [7, 8] or large intelligent surfaces (LISs) [9], have been proposed as an effective solution for overcoming signal blockage and enhancing the communication quality. An IRS is a thin man-made surface consisting of a large number of low-cost and passive reflecting elements, each of which can reflect and impact the propagation of an incident electromagnetic wave [6]. As a result, IRSs can create a *programmable wireless environment*. If the signal transmission via the direct link is blocked, an IRS can be deployed to provide an additional reflected link, hence improving the received signal strength. As the IRS does not require radio frequency (RF) chains and only reflects the incident signal in a nearly passive manner, it is more cost- and energy-efficient than conventional relaying technologies such as amplify-and-forward (AF) and decode-and-forward (DF) relaying [10]. Furthermore, IRSs can be easily deployed on different structures, such as building facades and roadside billboards in outdoor environments, as well as walls and ceilings in indoor environments.

A. Prior Works

1) *Robot Path Planning*: For the application of robots, path planning is essential for robots to carry out tasks reliably and safely. Hence, the robot path planning problem has been studied extensively in the past few decades. To ensure that robots will not collide with obstacles in their workspace, prior studies on robot path planning have proposed different algorithms for different application scenarios. By discretizing the continuous space into a finite grid, efficient robot path planning algorithms, including the Dijkstra, A*, and D* algorithms, were developed to find the shortest path between two locations in static and dynamic environments [11]. To cope with the more stringent challenges introduced by uncertain environments, the authors of [12] proposed a particle swarm optimization (PSO) based robot path planning algorithm. The authors of [13] investigated the multi-robot path planning problem and proposed an artificial bee colony optimization algorithm to minimize the sum path length of all robots. Exploiting machine learning, the authors of [14] invoked deep reinforcement learning for collision avoidance.

2) *IRS-assisted Communication System Design*: IRSs have received extensive attention from both academia and industry recently. By exploiting the new degrees of freedom introduced by passive beamforming, the performance gain facilitated by IRSs in wireless communication systems has been extensively investigated. For instance, the authors of [15] proposed an alternating optimization based algorithm for the design of the active beamforming at the BS and the passive beamforming at the IRS with the objective of minimizing the transmit power. The authors of [16] investigated energy-efficiency maximization in an IRS-assisted multiple-user multiple-

input single-output (MISO) system. In [17], the authors studied the physical layer security in IRS-aided communication systems, where the system sum secrecy rate was maximized. In [18], the authors considered an indoor IRS communication scenario, where the IRS phase shifts were configured by the proposed deep learning method to maximize the user's received signal strength. The authors of [19] focused on a multi-cell multiple-input multiple-output (MIMO) multiple-user communication system, where an IRS was deployed at the cell boundary to improve the performance of the cell-edge users. Furthermore, the authors of [20] invoked deep reinforcement learning techniques to tackle the joint active and passive beamforming problem. The proposed algorithm was shown to be capable of learning from the environment. In [21], the authors investigated IRS-assisted unmanned aerial vehicle (UAV) communication, where the UAV trajectory and the IRS phase shifts were jointly optimized to maximize the average achievable rate of a ground user. To further improve spectrum efficiency, non-orthogonal multiple access (NOMA) was considered for IRS-assisted communication systems. The authors of [22] analyzed various system performance metrics in an IRS-aided NOMA system, and provided useful design insights. With the aim of maximizing the system sum rate, joint active and passive beamforming optimization was investigated in [23] for IRS-assisted MISO NOMA communication systems.

B. Motivations and Challenges

On the road to facilitating smart cities and factories, connected robots have been regarded as an appealing technology. By offloading tasks to remote operators (e.g., BSs or APs), the cost and energy consumption of robots can be significantly reduced. However, as mentioned earlier, signal blockage is a major bottleneck for connected robots. Motivated by this issue, we propose to deploy an IRS to assist the communication with a connected robot. In particular, an IRS-enhanced indoor connected robot navigation system is considered, where one mobile robotic user (MRU) is served by an AP with the aid of an IRS, see Fig. 1. The MRU is dispatched to travel from a predefined initial location to a final location to carry out a specific mission. During the travel, the MRU's instantaneous communication quality should not fall below a certain threshold to prevent the loss of control. Although the performance gain introduced by IRSs has been studied for various wireless communication system architectures, to the best of the authors' knowledge, this is the first work to investigate the communication-aware indoor robot path planning problem in IRS-enhanced environments. The main related challenges are as follows:

- As the wireless link may be blocked by obstacles, as illustrated in Fig. 1, the communication quality of the MRU may change abruptly as it travels. This makes the considered

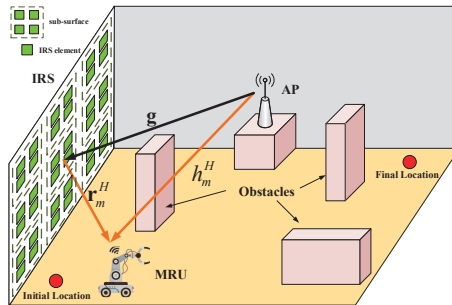


Fig. 1: Illustration of the IRS-enhanced indoor robot navigation system for a single-user scenario.

communication-aware indoor robot path planning problem more challenging than the conventional robot path planning problem which is only concerned with collision avoidance.

- In addition, the communication quality of the MRU does not only depend on its location but also on the IRS phase shifts, which causes the path planning and the IRS reflection matrix design to be highly coupled.

To overcome the aforementioned challenges, we develop a new radio-map based approach for the robot path planning problem. In general, a radio map contains information on the spectral activities and the propagation conditions in the space, frequency, and time domains [24]. This information can be exploited to improve the performance of wireless networks and facilitates new wireless applications. Inspired by this, we construct two types of radio maps, namely, a *channel power gain map* and a *communication rate map* for single-user and multiple-user scenarios, respectively, where we exploit knowledge about the channel propagation conditions. In the single-user case, one MRU is assumed to be served by the AP in a dedicated resource block with the aid of an IRS. As the communication performance is fully determined by the channel quality, a channel power gain map is constructed to characterize the maximum expected channel power gain of the MRU in the region of interest. In the multiple-user case, we consider one MRU and one static robotic user (SRU) which are simultaneously served by the AP. The communication performance of the robotic users also depends on the resource allocation at the AP. Hence, we construct a communication rate map, which characterizes the spatial distribution of the maximum expected rate of the MRU. Here, we jointly consider the MRU's location, the power allocation at the AP, and the phase shifts at the IRS. Equipped with the two radio maps, the communication-aware robot path planning problem is efficiently solved by utilizing graph theory.

C. Contributions

The main contributions of this paper can be summarized as follows:

- We propose an IRS-enhanced indoor robot navigation system, in which the IRS is deployed to enhance the signal transmission from the AP to an MRU. We formulate a communication-aware path planning problem to minimize the time/distance needed by the MRU for travelling from an initial to a final location. In particular, we jointly optimize the robot path and the IRS reflection matrix. *Radio map* [24] based approaches are proposed for both single-user and multiple-user systems.
- For the single-user scenario, we first construct the *channel power gain map* by optimizing the IRS phase shifts. The obtained channel power gain map characterizes the spatial distribution of the maximum expected effective channel power gain of the MRU aided by the IRS. Leveraging this map, the robot path planning problem is efficiently solved using graph theory.
- For the multiple-user scenario, we consider both NOMA and orthogonal multiple access (OMA) transmission schemes for simultaneously serving one MRU and one SRU. The *communication rate map* of the MRU is constructed by jointly optimizing the power allocation at the AP and the reflection matrix at the IRS, subject to the rate constraint of the SRU. Specifically, we solve the resulting joint optimization problem by invoking the bisection search and successive convex approximation (SCA) methods. Based on the rate map, a graph theory based solution for the path of the MRU is obtained.
- We show that the proposed IRS-enhanced system can significantly reduce the travelling distance of the MRU while achieving a higher communication rate compared to conventional systems without IRS. We also show that NOMA outperforms OMA, especially for the IRS-enhanced system.

D. Organization and Notation

The rest of this paper is organized as follows: In Section II, IRS-enhanced indoor robot path planning for a single-user system is investigated, and a channel power gain map is constructed for solving the formulated problem. In Section III, the robot path planning problem is extended to multiple-user systems for both NOMA and OMA transmission, and a communication rate map is constructed. Numerical examples are presented in Section IV to verify the effectiveness of the proposed designs compared to benchmark schemes. Finally, Section VI concludes the paper.

Notations: Scalars, vectors, and matrices are denoted by lower-case, bold-face lower-case, and bold-face upper-case letters, respectively. $\mathbb{C}^{N \times 1}$ denotes the space of $N \times 1$ complex-

valued vectors. The transpose and conjugate transpose of vector \mathbf{a} are denoted by \mathbf{a}^T and \mathbf{a}^H , respectively. $\|\mathbf{a}\|_1$ and $\|\mathbf{a}\|$ denote the 1-norm and the Euclidean norm of vector \mathbf{a} , respectively. $\text{diag}(\mathbf{a})$ denotes a diagonal matrix with the elements of vector \mathbf{a} on the main diagonal. $\mathbf{1}_{m \times n}$ denotes an all-one matrix of size $m \times n$. \mathbb{H}^N denotes the set of all N -dimensional complex Hermitian matrices. $\text{rank}(\mathbf{A})$ and $\text{Tr}(\mathbf{A})$ denote the rank and the trace of matrix \mathbf{A} , respectively. $\mathbf{A} \succeq 0$ indicates that \mathbf{A} is a positive semidefinite matrix. \otimes denotes the Kronecker product. $[\cdot]_n$ denotes the n th element of a vector.

II. RADIO MAP BASED ROBOT PATH PLANNING FOR SINGLE-USER SYSTEM

A. System Model

In this section, we consider an IRS-enhanced indoor robot navigation system, which consists of one single-antenna AP, one single-antenna MRU, and one IRS with M passive reflecting elements, see Fig. 1. The IRS is deployed on one of the indoor walls for assisting the transmission from the AP to the robotic user. Adopting a three-dimensional (3D) Cartesian coordinate system, the locations of the antenna of the AP and the center of the IRS are denoted by $\mathbf{b} = (x_b, y_b, H_b)$ and $\mathbf{f} = (x_f, y_f, H_f)$, respectively. The MRU is dispatched to travel from an initial location $\mathbf{q}_I = (x_I, y_I, H_0)$ to a final location $\mathbf{q}_F = (x_F, y_F, H_0)$, where H_0 denotes the height of the antenna of the MRU. Let $\mathbf{q}(t) = (x(t), y(t), H_0)$, $t \in [0, T]$, denote the time-varying path of the MRU, where T denotes the required travelling time¹. For practical implementation, the IRS is equipped with a smart controller, realized, e.g., with a field-programmable gate array (FPGA), which allows the AP to configure the IRS phase shifts in a real time manner. As the AP-IRS-user link suffers from severe path loss, a large number of reflecting elements are required for this link to achieve a comparable path loss as the unobstructed direct AP-user link [25]. However, a large number of reflecting elements also cause a prohibitively high overhead/complexity for channel acquisition and phase shift design/reconfiguration. To overcome this limitation, an effective method is to group adjacent reflecting elements, which are expected to experience high channel correlation, together to a sub-surface, as was done in [26]. All elements belonging to the same sub-surface are assumed to share the same reflection coefficient. In this paper, the M passive reflecting elements of the IRS are divided into N sub-surfaces, where each sub-surface consists of $\bar{N} = M/N$ reflecting

¹The considered setup is representative for many practical connected robot applications, such as transportation of material in smart factories or delivery of medicine in hospitals.

elements. An example where $\overline{N} = 4$ elements are grouped into a sub-surface is illustrated in Fig. 1. The instantaneous IRS reflection matrix is denoted by $\Theta(t) = \text{diag}(\boldsymbol{\theta}(t) \otimes \mathbf{1}_{\overline{N} \times 1}) \in \mathbb{C}^{M \times M}$, where $\boldsymbol{\theta}(t) = [\beta_1(t) e^{j\theta_1(t)}, \beta_2(t) e^{j\theta_2(t)}, \dots, \beta_N(t) e^{j\theta_N(t)}]^T$, and $\theta_n(t)$ and $\beta_n(t)$ denote the instantaneous phase shift and attenuation coefficient of the n th sub-surface of the IRS, respectively. In this paper, we assume $\theta_n(t) \in [0, 2\pi)$ and $\beta_n(t) = 1, \forall n \in \mathcal{N}, t \in \mathcal{T}$, where $\mathcal{N} = \{1, \dots, N\}$ and $\mathcal{T} = [0, T]$.

We focus our attention on the downlink transmission from the AP to the MRU. The channel between the AP and the IRS is denoted by $\mathbf{g} \in \mathbb{C}^{M \times 1}$, and follows the Rician channel model. Hence, \mathbf{g} can be expressed as

$$\mathbf{g} = \frac{\sqrt{\mathcal{L}_{AI}}}{\sqrt{K_{AI} + 1}} \left(\sqrt{K_{AI}} \overline{\mathbf{g}} + \widehat{\mathbf{g}} \right), \quad (1)$$

where \mathcal{L}_{AI} is the distance-dependent path loss of the AP-IRS channel, $\overline{\mathbf{g}}$ denotes the deterministic line-of-sight (LoS) component, $\widehat{\mathbf{g}}$ denotes the random non-LoS (NLoS) component, which follows the Rayleigh distribution, and K_{AI} is the Rician factor.

Furthermore, let $h_m(\mathbf{q}(t)) \in \mathbb{C}^{1 \times 1}$ and $\mathbf{r}_m(\mathbf{q}(t)) \in \mathbb{C}^{M \times 1}$ denote the AP-MRU and IRS-MRU channels for MRU location $\mathbf{q}(t)$. We have

$$h_m(\mathbf{q}(t)) = \frac{\sqrt{\mathcal{L}_{AM}(\mathbf{q}(t))}}{\sqrt{K_{AM}(\mathbf{q}(t)) + 1}} \left(\sqrt{K_{AM}(\mathbf{q}(t))} \overline{h}_m(\mathbf{q}(t)) + \widehat{h}_m \right), \quad (2)$$

$$\mathbf{r}_m(\mathbf{q}(t)) = \frac{\sqrt{\mathcal{L}_{IM}(\mathbf{q}(t))}}{\sqrt{K_{IM}(\mathbf{q}(t)) + 1}} \left(\sqrt{K_{IM}(\mathbf{q}(t))} \overline{\mathbf{r}}_m(\mathbf{q}(t)) + \widehat{\mathbf{r}}_m \right), \quad (3)$$

where $\mathcal{L}_{AM}(\mathbf{q}(t))$ and $\mathcal{L}_{IM}(\mathbf{q}(t))$ denote the corresponding path losses. $\overline{h}_m(\mathbf{q}(t))$ and $\overline{\mathbf{r}}_m(\mathbf{q}(t))$ are the location-dependent LoS components. \widehat{h}_m and $\widehat{\mathbf{r}}_m$ denote the random Rayleigh distributed NLoS components. $K_{AM}(\mathbf{q}(t))$ and $K_{IM}(\mathbf{q}(t))$ denote the location-dependent Rician factors. For instance, if the wireless link between the MRU at location $\mathbf{q}(t)$ and the AP/IRS is blocked by obstacles, the corresponding channel is classified as NLoS and we have $K_{AM/IM}(\mathbf{q}(t)) = 0^2$. Otherwise, it is classified as an LoS dominated channel and $K_{AM/IM}(\mathbf{q}(t)) = \kappa_{AM/IM}$, where $\kappa_{AM/IM}$ is a constant.

Due to the high path loss, similar to [15], signals that are reflected by the IRS two or more times are ignored. Therefore, the IRS-aided effective channel between the AP and the MRU can

²Note that, in practice, even if the direct LoS link is blocked, some of its energy may be reflected by the ceiling, floor, as well as walls and arrive at the receiver. However, we ignore the LoS link energy reflected by objects other than the IRS, which is a worst-case assumption for actual communication system design. Nevertheless, the results of this paper can be readily extended to the scenario with non-negligible reflected LoS links by adopting the corresponding channel models for radio map design.

be expressed as

$$c_m(t) = h_m^H(\mathbf{q}(t)) + \mathbf{r}_m^H(\mathbf{q}(t)) \Theta(t) \mathbf{g}. \quad (4)$$

We note that $c_m(t)$ is a random variable since it depends on random variables $\{\widehat{\mathbf{g}}, \widehat{\mathbf{r}}_m, \widehat{h}_m\}$. In this paper, we are interested in the expected/average effective channel power gain, defined as $\mathbb{E}[|c_m(t)|^2]$. A closed-form expression for $\mathbb{E}[|c_m(t)|^2]$ is provided in the following lemma.

Lemma 1. The expected effective channel power gain of the MRU is given by

$$\begin{aligned} \mathbb{E}[|c_m(t)|^2] \triangleq \lambda_m(t) &= \left| \widetilde{h}_m^H(\mathbf{q}(t)) + \widetilde{\mathbf{r}}_m^H(\mathbf{q}(t)) \Theta(t) \widetilde{\mathbf{g}} \right|^2 \\ &+ \frac{\mathcal{L}_{AM}(\mathbf{q}(t))}{K_{AM}(\mathbf{q}(t))+1} + \frac{\mathcal{L}_{AI} \mathcal{L}_{IM}(\mathbf{q}(t)) (K_{IM}(\mathbf{q}(t)) + K_{AI} + 1) M}{(K_{AI} + 1) (K_{IM}(\mathbf{q}(t)) + 1)}, \end{aligned} \quad (5)$$

where $\widetilde{h}_m^H(\mathbf{q}(t)) = \sqrt{\frac{\mathcal{L}_{AM}(\mathbf{q}(t)) K_{AM}(\mathbf{q}(t))}{K_{AM}(\mathbf{q}(t)) + 1}} \overline{h}_m^H(\mathbf{q}(t))$, $\widetilde{\mathbf{r}}_m^H(\mathbf{q}(t)) = \sqrt{\frac{\mathcal{L}_{IM}(\mathbf{q}(t)) K_{IM}(\mathbf{q}(t))}{K_{IM}(\mathbf{q}(t)) + 1}} \overline{\mathbf{r}}_m^H(\mathbf{q}(t))$, $\widetilde{\mathbf{g}} = \sqrt{\frac{\mathcal{L}_{AI} K_{AI}}{K_{AI} + 1}} \overline{\mathbf{g}}$.

Proof. See Appendix A. □

Based on **Lemma 1**, the calculation of $\lambda_m(t)$ requires the statistical channel state information (S-CSI) of each link, which can be obtained as follows: First, the instantaneous CSI (I-CSI) of each link is estimated several times via one of the recently proposed CSI estimation methods for IRS [26, 27]. Then, exploiting the estimated I-CSI, the S-CSI is obtained by employing standard mean and covariance matrix estimation techniques [28, 29]. For ease of exposition, let $\mathbf{w}_m^H(\mathbf{q}(t)) = \widetilde{\mathbf{r}}_m^H(\mathbf{q}(t)) \text{diag}(\widetilde{\mathbf{g}}) \in \mathbb{C}^{1 \times M}$ denote the cascaded LoS channel of the AP-IRS-MRU link before the reconfiguration of the IRS. Then, the corresponding combined composite channel associated with the n th sub-surface is given by $[\widetilde{\mathbf{w}}_m^H(\mathbf{q}(t)) \in \mathbb{C}^{1 \times N}]_n = \sum_{\overline{n}=1}^{\overline{N}} [\mathbf{w}_m^H(\mathbf{q}(t))]_{\overline{n}+(n-1)\overline{N}}, \forall n \in \mathcal{N}$ [26]. Therefore, $\lambda_m(t)$ can be rewritten as

$$\begin{aligned} \lambda_m(t) &= \left| \widetilde{h}_m^H(\mathbf{q}(t)) + \mathbf{w}_m^H(\mathbf{q}(t)) (\boldsymbol{\theta}(t) \otimes \mathbf{1}_{\overline{N} \times 1}) \right|^2 + \tau_m(\mathbf{q}(t)) \\ &= \left| \widetilde{h}_m^H(\mathbf{q}(t)) + \widetilde{\mathbf{w}}_m^H(\mathbf{q}(t)) \boldsymbol{\theta}(t) \right|^2 + \tau_m(\mathbf{q}(t)), \end{aligned} \quad (6)$$

where $\tau_m(\mathbf{q}(t)) = \frac{\mathcal{L}_{AM}(\mathbf{q}(t))}{K_{AM}(\mathbf{q}(t))+1} + \frac{\mathcal{L}_{AI} \mathcal{L}_{IM}(\mathbf{q}(t)) (K_{IM}(\mathbf{q}(t)) + K_{AI} + 1) M}{(K_{AI} + 1) (K_{IM}(\mathbf{q}(t)) + 1)}$.

B. Problem Formulation

We aim to minimize the required travelling time T of the MRU from \mathbf{q}_I to \mathbf{q}_F by jointly optimizing the path of the MRU, $Q = \{\mathbf{q}(t), 0 \leq t \leq T\}$, and the reflection matrix of the IRS

$A = \{\Theta(t), 0 \leq t \leq T\}$, subject to a constraint on the expected effective channel power gain.

Hence, the communication-aware robot path planning problem can be formulated as

$$\min_{Q,A,T} T \quad (7a)$$

$$\text{s.t. } \lambda_m(t) \geq \bar{\gamma}, \forall t \in \mathcal{T}, \quad (7b)$$

$$\theta_n(t) \in [0, 2\pi), \forall n \in \mathcal{N}, t \in \mathcal{T}, \quad (7c)$$

$$\mathbf{q}(0) = \mathbf{q}_I, \mathbf{q}(T) = \mathbf{q}_F, \quad (7d)$$

$$\|\dot{\mathbf{q}}(t)\| \leq V_{\max}, \forall t \in \mathcal{T}, \quad (7e)$$

where the first derivative of $\mathbf{q}(t)$ with respect to t , $\dot{\mathbf{q}}(t)$, denotes the velocity vector, and $\bar{\gamma}$ denotes the minimum required expected effective channel power gain, which has to be achieved throughout the travel of the MRU. Constraints (7d) and (7e) represent the mobility constraints on the MRU, where V_{\max} is the maximum travelling speed. Problem (7) is challenging to solve for the following three reasons. Firstly, constraint (7b) is not concave with respect to $\mathbf{q}(t)$ and $\Theta(t)$. The unit modulus constraint (7c) is also non-convex. Secondly, the expected effective channel power gain $\lambda_m(t)$ is generally not a continuous function under the considered location-dependent channel model. Thirdly, problem (7) involves an infinite number of optimization variables with respect to continuous time t , which are difficult to handle. To tackle these difficulties, we develop a radio map based approach which is capable of exploiting knowledge regarding location-dependent channel propagation.

C. Channel Power Gain Map Construction

In this subsection, we introduce a specific type of radio map, namely, the channel power gain map. Specifically, the channel power gain map characterizes the spatial distribution of the expected effective channel power gain over the region of interest with respect to the MRU's location \mathbf{q} , i.e., $\lambda_m(\mathbf{q})$. Let \bar{X} and \bar{Y} denote the range of the two-dimensional (2D) space along the x-axis and y-axis, respectively. For the development of the radio map, the continuous 2D space is first discretized into $\frac{\bar{X}}{\Delta_x} \times \frac{\bar{Y}}{\Delta_y}$ small cells, where Δ_x and Δ_y denote the resolution of the radio map along the x-axis and y-axis, respectively, which should be chosen such that the location of the MRU within each cell can be approximated by the cell center. To guarantee a certain desired accuracy of the approximation, the values of Δ_x and Δ_y can be selected such

that $\Delta_x \leq \varepsilon \bar{X}$ and $\Delta_y \leq \varepsilon \bar{Y}$, where ε is a predefined threshold for the accuracy³. The horizontal location of the (i, j) -th cell center can be expressed as

$$\mathbf{q}_{i,j}^\Delta = \mathbf{q}_0 + [(i-1)\Delta_x, (j-1)\Delta_y], i \in \mathcal{X}, j \in \mathcal{Y}, \quad (8)$$

where \mathbf{q}_0 is the center of the cell in the lower left corner of the considered 2D space, $\mathcal{X} = \{1, \dots, X\}$, $\mathcal{Y} = \{1, \dots, Y\}$, $X \triangleq \frac{\bar{X}}{\Delta_x}$, and $Y \triangleq \frac{\bar{Y}}{\Delta_y}$.

Accordingly, let matrix $\mathbf{C} \in \mathbb{R}^{X \times Y}$ denote the channel power gain map, where the element in row i and column j characterizes the maximum expected effective channel power gain of the MRU at location $\{\mathbf{q}_{i,j}^\Delta\}$. Therefore, the elements of \mathbf{C} are given by

$$[\mathbf{C}]_{i,j} = \max_{\Theta \in \mathcal{F}} \left| \tilde{h}_m^H(\mathbf{q}_{i,j}^\Delta) + \tilde{\mathbf{w}}_m^H(\mathbf{q}_{i,j}^\Delta) \boldsymbol{\theta}(\mathbf{q}_{i,j}^\Delta) \right|^2 + \tau_m(\mathbf{q}_{i,j}^\Delta), i \in \mathcal{X}, j \in \mathcal{Y}, \quad (9)$$

where \mathcal{F} denotes the set of all possible IRS reflection matrices.

For any given $\mathbf{q}_{i,j}^\Delta$, the expected effective channel power gain is upper-bounded by

$$\left| \tilde{h}_m^H(\mathbf{q}_{i,j}^\Delta) + \tilde{\mathbf{w}}_m^H(\mathbf{q}_{i,j}^\Delta) \boldsymbol{\theta} \right|^2 + \tau_m(\mathbf{q}_{i,j}^\Delta) \leq \left(\left| \tilde{h}_m^H(\mathbf{q}_{i,j}^\Delta) \right| + \left\| \tilde{\mathbf{w}}_m^H(\mathbf{q}_{i,j}^\Delta) \right\|_1 \right)^2 + \tau_m(\mathbf{q}_{i,j}^\Delta). \quad (10)$$

The above inequality holds with equality for the following optimal phase shifts:

$$\theta_n^*(\mathbf{q}_{i,j}^\Delta) = \angle \left(\tilde{h}_m^H(\mathbf{q}_{i,j}^\Delta) \right) - \angle \left([\tilde{\mathbf{w}}_m^H(\mathbf{q}_{i,j}^\Delta)]_n \right), \forall n \in \mathcal{N}, \quad (11)$$

where $\angle(\cdot)$ denotes the phase of a complex number. Therefore, the channel power gain map \mathbf{C} is given as follows:

$$[\mathbf{C}]_{i,j} = \left(\left| \tilde{h}_m^H(\mathbf{q}_{i,j}^\Delta) \right| + \left\| \tilde{\mathbf{w}}_m^H(\mathbf{q}_{i,j}^\Delta) \right\|_1 \right)^2 + \tau_m(\mathbf{q}_{i,j}^\Delta), i \in \mathcal{X}, j \in \mathcal{Y}. \quad (12)$$

³Though small values of ε (i.e., small Δ_x and Δ_y) increase the accuracy of the approximation, they also cause a high computational complexity for robot path planning due to the resulting large number of cells. In practice, ε has to be properly chosen to balance between accuracy and complexity.

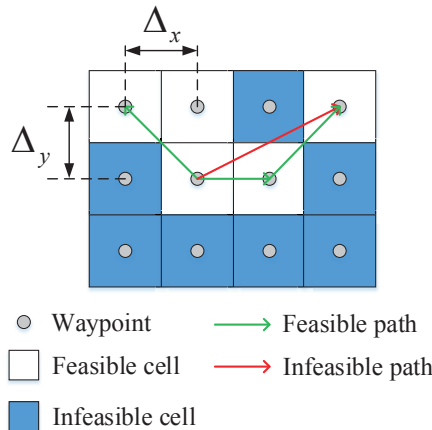


Fig. 2: Illustration of path structure for problem (13).

D. Graph Theory Based Path Solution

Based on the constructed channel power gain map, let $Q = \{\mathbf{q}_{i_1, j_1}^\Delta, \mathbf{q}_{i_2, j_2}^\Delta, \dots, \mathbf{q}_{i_{D-1}, j_{D-1}}^\Delta, \mathbf{q}_{i_D, j_D}^\Delta\}$ denote the path of the MRU. For ease of exposition, we assume that $\mathbf{q}_{i_1, j_1}^\Delta = \mathbf{q}_I$ and $\mathbf{q}_{i_D, j_D}^\Delta = \mathbf{q}_F$. It can be verified that for the optimal solution of (7), the speed constraint (7e) must be satisfied with equality, i.e., $\|\dot{\mathbf{q}}(t)\| = V_{\max}, \forall t \in \mathcal{T}$. To demonstrate this, suppose that for the optimal solution to problem (7), the MRU travels at a speed strictly less than V_{\max} . Then, we can increase the speed to V_{\max} , which decreases the travelling time. With this insight, problem (7) can be equivalently reformulated as the following *travelling distance minimization* problem over the channel power gain map:

$$\min_{Q, D} \sum_{d=1}^{D-1} \left\| \mathbf{q}_{i_{d+1}, j_{d+1}}^\Delta - \mathbf{q}_{i_d, j_d}^\Delta \right\| \quad (13a)$$

$$\text{s.t. } [\mathbf{C}]_{i_d, j_d} \geq \bar{\gamma}, \quad (13b)$$

$$\left\| \mathbf{q}_{i_{d+1}, j_{d+1}}^\Delta - \mathbf{q}_{i_d, j_d}^\Delta \right\| \leq \sqrt{\Delta_x^2 + \Delta_y^2}, 1 \leq d \leq D-1, \quad (13c)$$

$$\mathbf{q}_{i_1, j_1}^\Delta = \mathbf{q}_I, \mathbf{q}_{i_D, j_D}^\Delta = \mathbf{q}_F, \quad (13d)$$

where (13c) ensures that any two successive waypoints along the path are adjacent in the channel power gain map. As illustrated in Fig. 2, if the two successive waypoints satisfy the expected effective channel power gain condition, it is guaranteed that any point on the line segment connecting them also satisfies this condition (e.g., green lines). Otherwise, if the two successive waypoints were not adjacent, the path may not be always feasible (e.g., the red line). However, problem (13) is a non-convex combinatorial optimization problem, which is difficult to solve with standard convex optimization methods. In the following, we solve problem (13) by exploiting graph theory [30].

For given $\bar{\gamma}$ and channel power gain map \mathbf{C} , we construct a new matrix $\mathbf{\Pi} \in \mathbb{R}^{\mathcal{X} \times \mathcal{Y}}$, namely the feasible map, as follows:

$$[\mathbf{\Pi}]_{i,j} = \begin{cases} 1, & \text{if } [\mathbf{C}]_{i,j} \geq \bar{\gamma} \\ 0, & \text{otherwise} \end{cases}, i \in \mathcal{X}, j \in \mathcal{Y}. \quad (14)$$

Specifically, $[\mathbf{\Pi}]_{i,j} = 1$ means that the location $\mathbf{q}_{i,j}^\Delta$ is a feasible candidate waypoint for the path of the MRU.

Based on the feasible map $\mathbf{\Pi}$, we construct an undirected weighted graph, which is denoted by $G = (V, E)$. The vertex set V and the edge set E are given by

$$V = \left\{ \mathbf{v}_{i,j} = \mathbf{q}_{i,j}^{\Delta} : [\mathbf{\Pi}]_{i,j} = 1, i \in \mathcal{X}, j \in \mathcal{Y} \right\}, \quad (15a)$$

$$E = \{ (\mathbf{v}_{i,j}, \mathbf{v}_{i',j'}) : \mathbf{v}_{i,j}, \mathbf{v}_{i',j'} \in V \}. \quad (15b)$$

The weight of each edge is denoted by $W(\mathbf{v}_{i,j}, \mathbf{v}_{i',j'})$, and given by

$$W(\mathbf{v}_{i,j}, \mathbf{v}_{i',j'}) = \begin{cases} \|\mathbf{v}_{i,j} - \mathbf{v}_{i',j'}\|, & \text{if } \|\mathbf{v}_{i,j} - \mathbf{v}_{i',j'}\| \leq \sqrt{\Delta_x^2 + \Delta_y^2} \\ \infty, & \text{otherwise} \end{cases}. \quad (16)$$

Based on the constructed graph G , problem (13) is equivalent to finding the shortest path from $\mathbf{v}_{i_1, j_1} = \mathbf{q}_I$ to $\mathbf{v}_{i_D, j_D} = \mathbf{q}_F$. The shortest path construction problem can be efficiently solved via the Dijkstra algorithm [30] with complexity $\mathcal{O}(|V|^2)$. The optimal path for the MRU is denoted by $Q^* = \left\{ \mathbf{q}_{i_1, j_1}^{*\Delta}, \mathbf{q}_{i_2, j_2}^{*\Delta}, \dots, \mathbf{q}_{i_{D-1}, j_{D-1}}^{*\Delta}, \mathbf{q}_{i_D, j_D}^{*\Delta} \right\}$.

III. RADIO MAP BASED ROBOT PATH PLANNING FOR MULTIPLE-USER SYSTEM

A. System Model

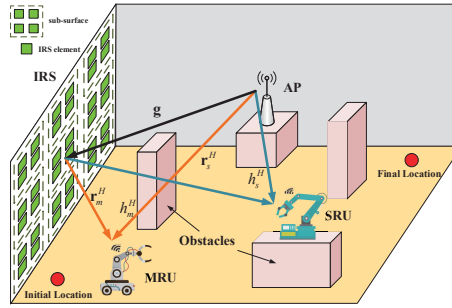


Fig. 3: Illustration of the IRS-enhanced indoor robot navigation system for a multiple-user scenario.

Different from the single-user scenario, where the MRU is assigned a dedicated resource block, we further investigate the scenario where multiple robotic users are simultaneously served by the AP. More particularly, two types of robotic users are considered, namely, an MRU and an SRU, as shown in Fig. 3⁴. The location of the SRU is denoted by $\mathbf{u}_s = (x_s, y_s, H_s)$. Since the location of the SRU is usually selected to avoid signal blockage and to avoid collisions with the MRU (e.g., by placing the SRU on a high work platform), Rician fading is assumed for the AP-SRU and IRS-SRU channels, respectively, which are modelled as follows:

$$h_s = \frac{\sqrt{\mathcal{L}_{AS}}}{\sqrt{K_{AS} + 1}} \left(\sqrt{K_{AS} \bar{h}_s} + \hat{h}_s \right), \quad (17)$$

⁴One practical scenario for the multiple-user setup is automatic industrial production in smart factories, where the MRU is used for transportation of materials, and the SRU is used for assembling products. Both users need to maintain a reliable communication link to ensure safe operation.

$$\mathbf{r}_s = \frac{\sqrt{\mathcal{L}_{IS}}}{\sqrt{K_{IS} + 1}} \left(\sqrt{K_{IS}} \bar{\mathbf{r}}_s + \hat{\mathbf{r}}_s \right), \quad (18)$$

where \mathcal{L}_{AS} and \mathcal{L}_{IS} denote the distance-dependent path losses, \bar{h}_s and $\bar{\mathbf{r}}_s$ denote the deterministic LoS components, and \hat{h}_s and $\hat{\mathbf{r}}_s$ denote the random NLoS components. K_{AS} and K_{IS} are the Rician factors.

Therefore, the effective channel from the AP to the SRU is given by $c_s(t) = h_s^H + \mathbf{r}_s^H \Theta(t) \mathbf{g}$. Similar to **Lemma 1** and (6), the expected effective channel power gain of the SRU can be expressed as

$$\begin{aligned} \mathbb{E} [|c_s(t)|^2] &= \left| \tilde{h}_s^H + \tilde{\mathbf{r}}_s^H \Theta(t) \tilde{\mathbf{g}} \right|^2 + \frac{\mathcal{L}_{AS}}{K_{AS} + 1} + \frac{\mathcal{L}_{AI} \mathcal{L}_{IS} (K_{IS} + K_{AI} + 1) M}{(K_{AI} + 1)(K_{IS} + 1)} \\ &= \left| \tilde{h}_s^H + \tilde{\mathbf{w}}_s^H \boldsymbol{\theta}(t) \right|^2 + \tau_s \triangleq \lambda_s(t), \end{aligned} \quad (19)$$

where $\tilde{h}_s^H = \sqrt{\frac{\mathcal{L}_{AS} K_{AS}}{K_{AS} + 1}} \bar{h}_s^H$, $\tilde{\mathbf{r}}_s^H = \sqrt{\frac{\mathcal{L}_{IS} K_{IS}}{K_{IS} + 1}} \bar{\mathbf{r}}_s^H$, $\mathbf{w}_s^H = \tilde{\mathbf{r}}_s^H \text{diag}(\tilde{\mathbf{g}}) \in \mathbb{C}^{1 \times M}$, $[\tilde{\mathbf{w}}_s^H \in \mathbb{C}^{1 \times N}]_n = \sum_{\bar{n}=1}^{\bar{N}} [\mathbf{w}_s^H]_{\bar{n} + (n-1)\bar{N}}$, $\forall n \in \mathcal{N}$, and $\tau_s = \frac{\mathcal{L}_{AS}}{K_{AS} + 1} + \frac{\mathcal{L}_{AI} \mathcal{L}_{IS} (K_{IS} + K_{AI} + 1) M}{(K_{AI} + 1)(K_{IS} + 1)}$.

Regarding the multiple access scheme applied at the AP for serving the two robotic users, both NOMA and OMA transmission are considered. In NOMA, the AP simultaneously serves the MRU and the SRU in the same time/frequency resource blocks by utilizing superposition coding (SC) and successive interference cancelation (SIC)⁵. For OMA, we focus on frequency division multiple access (FDMA), where the AP simultaneously serves the two users in different frequency resource blocks⁶.

1) NOMA: According to the NOMA protocol, the AP transmits the two users' signals using superposition coding. The received signal of user $l \in \{s, m\}$ at time instant t can be expressed as

$$e_l(t) = c_l(t) \left(\sqrt{p_s(t)} b_s(t) + \sqrt{p_m(t)} b_m(t) \right) + n_l(t), \quad (20)$$

where $b_s(t)$ and $b_m(t)$ are the transmitted data symbols for the SRU and the MRU, respectively, which are modelled as circularly symmetric complex Gaussian (CSCG) random variables with zero mean and unit variance. Let P_{\max} denote the maximum transmit power at the AP. The power allocation of the two users has to satisfy $p_s(t) + p_m(t) \leq P_{\max}, \forall t$. $n_l(t)$ denotes the additive CSCG noise at user $l \in \{s, m\}$ with zero mean and variance σ^2 .

By invoking SIC, the user with the stronger channel power gain is able to first decode the

⁵SC and SIC required for NOMA introduce additional complexity compared to OMA. However, on the other hand, NOMA yields a significant performance gain over OMA, see Section IV-B for details.

⁶For time division multiple access (TDMA), the AP needs to serve the two users consecutively in different time resource blocks, which causes transmission delays. Therefore, we consider FDMA to ensure a fair comparison with NOMA.

signal of the user with the weaker channel power gain, before decoding its own signal [31]. We define binary indicators $\mu_l(t) \in \{0, 1\}$, $l \in \{s, m\}$, to specify the instantaneous decoding order of the two users, which satisfy $\mu_m(t) + \mu_s(t) = 1, \forall t$. For instance, if the MRU is the strong user, we have $\mu_m(t) = 0$ and $\mu_s(t) = 1$. In this case, the effective channel power gain should satisfy $|c_m(t)|^2 \geq |c_s(t)|^2$ to ensure the success of SIC [31]. Therefore, the achievable communication rate of user $l \in \{s, m\}$ can be expressed as

$$R_l^{\text{NOMA}}(t) = \log_2 \left(1 + \frac{|c_l(t)|^2 p_l(t)}{\mu_l(t) |c_l(t)|^2 p_{\bar{l}}(t) + \sigma^2} \right) = \log_2 \left(1 + \frac{p_l(t)}{\mu_l(t) p_{\bar{l}}(t) + \frac{\sigma^2}{|c_l(t)|^2}} \right). \quad (21)$$

Here, if $l = m$, we have $\bar{l} = s$; otherwise, $\bar{l} = m$. Note that $R_l^{\text{NOMA}}(t)$ is a random variable, and we are interested in the expected/average achievable communication rate, defined as $\mathbb{E} [R_l^{\text{NOMA}}(t)]$. However, it is difficult to derive a closed-form expression for $\mathbb{E} [R_l^{\text{NOMA}}(t)]$, since its probability distribution is hard to obtain. To tackle this issue, we approximate the expected achievable communication rate by an upper bound as follows:

$$\mathbb{E} [R_l^{\text{NOMA}}(t)] \stackrel{(a)}{\leq} \log_2 \left(1 + \frac{p_l(t)}{\mu_l(t) p_{\bar{l}}(t) + \frac{\sigma^2}{\mathbb{E}[|c_l(t)|^2]}} \right) = \log_2 \left(1 + \frac{p_l(t)}{\mu_l(t) p_{\bar{l}}(t) + \frac{\sigma^2}{\lambda_l(t)}} \right) \triangleq \bar{R}_l^{\text{NOMA}}(t), \quad (22)$$

where (a) holds due to the Jensen's inequality since the rate function $R_l^{\text{NOMA}}(t)$ is concave with respect to $|c_l(t)|^2$ and $\{p_l(t)\}$ are deterministic variables which are selected by the AP, see Section III-B. The tightness of the approximation $\bar{R}_l^{\text{NOMA}}(t)$ with respect to the exact average rate $\mathbb{E} [R_l^{\text{NOMA}}(t)]$ will be evaluated in Section VI-B4.

2) *OMA*: For OMA transmission, the AP simultaneously transmits to both users in orthogonal frequency bands of equal size. Accordingly, the achievable communication rate for user $l \in \{s, m\}$ is given by

$$R_l^{\text{OMA}}(t) = \frac{1}{2} \log_2 \left(1 + \frac{|c_l(t)|^2 p_l(t)}{\frac{1}{2} \sigma^2} \right). \quad (23)$$

Similarly, the expected achievable communication rate for OMA can be approximated as

$$\mathbb{E} [R_l^{\text{OMA}}(t)] \leq \frac{1}{2} \log_2 \left(1 + \frac{\mathbb{E} [|c_l(t)|^2] p_l(t)}{\frac{1}{2} \sigma^2} \right) = \frac{1}{2} \log_2 \left(1 + \frac{2\lambda_l(t) p_l(t)}{\sigma^2} \right) \triangleq \bar{R}_l^{\text{OMA}}(t), \quad (24)$$

B. Problem Formulation

For the multiple-user scenario, the communication-aware robot path planning problem is formulated as follows:

$$\min_{Q, P, A, T} T \quad (25a)$$

$$\text{s.t. } \bar{R}_l^Z(t) \geq \bar{r}_l, Z \in \{\text{NOMA}, \text{OMA}\}, l \in \{s, m\}, \forall t \in \mathcal{T}, \quad (25b)$$

$$p_l(t) \geq 0, l \in \{s, m\}, p_m(t) + p_s(t) \leq P_{\max}, \forall t \in \mathcal{T}, \quad (25c)$$

$$\mu_l(t) \in \{0, 1\}, l \in \{s, m\}, \forall t \in \mathcal{T}, \quad (25d)$$

$$\mu_m(t) + \mu_s(t) = 1, \forall t \in \mathcal{T}, \quad (25e)$$

$$\begin{cases} \lambda_s(t) \geq \lambda_m(t), \text{ if } \mu_s(t) = 0, \mu_m(t) = 1 \\ \lambda_s(t) \leq \lambda_m(t), \text{ otherwise} \end{cases}, \forall t \in \mathcal{T}, \quad (25f)$$

$$(7c) - (7e), \quad (25g)$$

where $P = \{p_m(t), p_s(t), 0 \leq t \leq T\}$ denotes the power allocation at the AP, $\bar{r}_l, l \in \{s, m\}$, denote the minimum required communication rate of MRU and SRU, and $Z \in \{\text{NOMA}, \text{OMA}\}$ indicates whether NOMA or OMA is employed. Constraint (25c) denotes the power allocation constraint. Constraints (25d)-(25f) ensure that SIC can be successfully implemented at the stronger user and is only valid when NOMA is used, i.e., $Z = \text{NOMA}$.

C. Communication Rate Map Construction

Different from the single-user scenario, where the communication performance of the MRU is only determined by its location and the IRS phase shifts, the communication performance in problem (25) is also determined by the power allocation at the AP. Moreover, the effective channels of the MRU and the SRU share the same IRS phase shifts, which makes problem (25) challenging to solve. To tackle this difficulty, we construct a different type of radio map, which we refer to as the *communication rate map* of the MRU, by jointly optimizing the power allocation at the AP and the phase shifts at the IRS.

1) *NOMA*: Let matrix $\mathbf{U}^{\text{NOMA}} \in \mathbb{R}^{X \times Y}$ denote the communication rate map for NOMA. The elements of \mathbf{U}^{NOMA} represent the maximum expected communication rates of the MRU at locations $\{\mathbf{q}_{i,j}^\Delta\}$, such that the communication rate requirement of the SRU is satisfied. Therefore, the element in row i and column j of \mathbf{U}^{NOMA} is given by

$$[\mathbf{U}^{\text{NOMA}}]_{i,j} = \max_{p_m, p_s, \boldsymbol{\Theta}, \mu_m, \mu_s, \bar{r}_0} \bar{r}_0 \quad (26a)$$

$$\text{s.t. } \bar{R}_m^{\text{NOMA}}(\mathbf{q}_{i,j}^\Delta) \geq \bar{r}_0, \quad (26b)$$

$$\bar{R}_s^{\text{NOMA}}(\mathbf{q}_{i,j}^\Delta) \geq \bar{r}_s, \quad (26c)$$

$$\theta_n \in [0, 2\pi), \forall n \in \mathcal{N}, \quad (26d)$$

$$p_l \geq 0, l \in \{s, m\}, p_m + p_s \leq P_{\max}, \quad (26e)$$

$$\mu_l \in \{0, 1\}, l \in \{s, m\}, \quad (26f)$$

$$\mu_m + \mu_s = 1, \quad (26g)$$

$$\begin{cases} \lambda_s \geq \lambda_m(\mathbf{q}_{i,j}^\Delta), \text{ if } \mu_s = 0, \mu_m = 1 \\ \lambda_s \leq \lambda_m(\mathbf{q}_{i,j}^\Delta), \text{ otherwise} \end{cases}, \quad (26h)$$

where \bar{r}_0 denotes the maximum expected communication rate of the MRU. Let \bar{r}_0^* denote the optimal solution of problem (26). As there are $2! = 2$ options for the decoding order for two users, we can solve problem (26) by exhaustively searching over all possible decoding order options, i.e., $\bar{r}_0^* = \arg \max_{k \in \{1,2\}} (\bar{r}_0^{k*})$, where \bar{r}_0^{k*} denotes the optimal solution of problem (26) for the k th decoding order option.

To solve problem (26), we first introduce auxiliary variables $\tilde{\mathbf{h}}_m^H = [\tilde{\mathbf{w}}_s^H(\mathbf{q}_{i,j}^\Delta) \tilde{h}_m^H(\mathbf{q}_{i,j}^\Delta)]$, $\tilde{\mathbf{h}}_s^H = [\tilde{\mathbf{w}}_s^H \tilde{h}_s^H]$, and $\mathbf{v} = [e^{j\theta_1}, e^{j\theta_2}, \dots, e^{j\theta_N}, 1]^T$. Moreover, we define $\tilde{\mathbf{H}}_l = \tilde{\mathbf{h}}_l \tilde{\mathbf{h}}_l^H$, $l \in \{s, m\}$, and $\mathbf{V} = \mathbf{v}\mathbf{v}^H$, which satisfies $\mathbf{V} \succeq 0$, $\text{rank}(\mathbf{V}) = 1$, and $[\mathbf{V}]_{nn} = 1, n = 1, 2, \dots, N+1$. Then, the expected effective channel power gain of the MRU and the SRU can be rewritten as

$$\lambda_m(\mathbf{q}_{i,j}^\Delta) = \left| \tilde{\mathbf{h}}_m^H \mathbf{v} \right|^2 + \tau_m(\mathbf{q}_{i,j}^\Delta) = \text{Tr}(\tilde{\mathbf{H}}_m \mathbf{V}) + \tau_m(\mathbf{q}_{i,j}^\Delta), \quad (27)$$

$$\lambda_s = \left| \tilde{\mathbf{h}}_s^H \mathbf{v} \right|^2 + \tau_s = \text{Tr}(\tilde{\mathbf{H}}_s \mathbf{V}) + \tau_s. \quad (28)$$

For a given user decoding order⁷, problem (26) can be reformulated as

$$\max_{p_m, p_s, \mathbf{V}, \bar{r}_0^k} \bar{r}_0^k \quad (29a)$$

$$\text{s.t. } \log_2 \left(1 + \frac{p_m}{p_s + \frac{\sigma^2}{\text{Tr}(\tilde{\mathbf{H}}_m \mathbf{V}) + \tau_m(\mathbf{q}_{i,j}^\Delta)}} \right) \geq \bar{r}_0^k, \quad (29b)$$

$$\log_2 \left(1 + \frac{p_s (\text{Tr}(\tilde{\mathbf{H}}_s \mathbf{V}) + \tau_s)}{\sigma^2} \right) \geq \bar{r}_s, \quad (29c)$$

$$\text{Tr}(\tilde{\mathbf{H}}_s \mathbf{V}) + \tau_s \geq \text{Tr}(\tilde{\mathbf{H}}_m \mathbf{V}) + \tau_m(\mathbf{q}_{i,j}^\Delta), \quad (29d)$$

$$[\mathbf{V}]_{nn} = 1, n = 1, 2, \dots, N+1, \quad (29e)$$

$$\mathbf{V} \succeq 0, \mathbf{V} \in \mathbb{H}^{N+1}, \quad (29f)$$

$$\text{rank}(\mathbf{V}) = 1, \quad (29g)$$

$$(26e). \quad (29h)$$

⁷Here, we consider the case where the SRU is the strong user, i.e., $\mu_s = 0, \mu_m = 1$. A similar problem can be also formulated for $\mu_s = 1, \mu_m = 0$.

Due to the non-convex constraints (29b), (29c), and (29g), problem (29) is a non-convex optimization problem, and hence, difficult to solve globally optimally. To address this issue, we develop an efficient bisection search based algorithm to derive a high-quality suboptimal solution. First, for a given rate target \bar{r}_0^t , the non-convex constraints (29b) and (29c) can be rearranged as

$$p_m \geq \left(2^{\bar{r}_0^t} - 1\right) \left(p_s + \frac{\sigma^2}{\text{Tr}(\tilde{\mathbf{H}}_m \mathbf{V}) + \tau_m(\mathbf{q}_{i,j}^\Delta)} \right), \quad (30)$$

$$\text{Tr}(\tilde{\mathbf{H}}_s \mathbf{V}) + \tau_s \geq \frac{(2^{\bar{r}_s} - 1) \sigma^2}{p_s}. \quad (31)$$

Then, we have the following feasibility check problem:

$$\max_{p_m, p_s, \mathbf{V}} 1 \quad (32a)$$

$$\text{s.t. (26e), (29d) - (29g), (30), (31).} \quad (32b)$$

For a given rate target \bar{r}_0^t , if problem (32) is feasible, it follows that $\bar{r}_0^{k*} \geq \bar{r}_0^t$, otherwise, $\bar{r}_0^{k*} < \bar{r}_0^t$. Therefore, problem (29) can be solved by successively checking the feasibility of problem (32) with updated \bar{r}_0^t 's until the bisection search terminates. However, problem (32) is non-convex due to the non-convex rank-one constraint (29g). To handle this difficulty, we first transform rank constraint (29g) equivalently into the follow constraint:

$$\|\mathbf{V}\|_* - \|\mathbf{V}\|_2 \leq 0, \quad (33)$$

where $\|\mathbf{V}\|_* = \sum_i \sigma_i(\mathbf{V})$ and $\|\mathbf{V}\|_2 = \sigma_1(\mathbf{V})$ denote the nuclear norm and spectral norm, respectively, and $\sigma_i(\mathbf{V})$ is the i th largest singular value of matrix \mathbf{V} . For any $\mathbf{V} \in \mathbb{H}^{N+1}$, we have $\|\mathbf{V}\|_* - \|\mathbf{V}\|_2 \geq 0$ and equality holds if and only if \mathbf{V} is a rank-one matrix. Therefore, the feasibility of problem (32) can be checked by solving the following problem:

$$\min_{p_m, p_s, \mathbf{V}} \|\mathbf{V}\|_* - \|\mathbf{V}\|_2 \quad (34a)$$

$$\text{s.t. (26e), (29d) - (29f), (30), (31).} \quad (34b)$$

Specifically, if the objective function of problem (34) is zero, it means that a rank-one solution can be obtained and problem (32) is feasible, otherwise, problem (32) is infeasible. However, problem (34) is still non-convex due to the non-convex objective function. In the following, we invoke SCA [32] to find a suboptimal solution of (34) iteratively.

As the objective function of (34) is a difference of convex (DC) functions, for a given feasible point $\mathbf{V}^{\tilde{n}}$ in the \tilde{n} th iteration of the SCA method, a lower bound on $\|\mathbf{V}\|_2$ is constructed via a first-order Taylor expansion as follows:

$$\|\mathbf{V}\|_2 \geq \|\mathbf{V}^{\tilde{n}}\|_2 + \text{Tr} \left[\mathbf{u}_{\max}(\mathbf{V}^{\tilde{n}}) (\mathbf{u}_{\max}(\mathbf{V}^{\tilde{n}}))^H (\mathbf{V} - \mathbf{V}^{\tilde{n}}) \right] \triangleq \bar{\mathbf{V}}^{\tilde{n}}, \quad (35)$$

Algorithm 1 SCA based Algorithm for Problem (34)

- 1: Initialize \mathbf{V}^0 , and set iteration index $\tilde{n} = 0$.
 - 2: **repeat**
 - 3: Solve problem (36) for given $\mathbf{V}^{\tilde{n}}$.
 - 4: Update $\mathbf{V}^{\tilde{n}+1}$ with the obtained optimal solution, and $\tilde{n} = \tilde{n} + 1$.
 - 5: **until convergence**
 - 6: Return the converged objective function of (36).
- where $\mathbf{u}_{\max}(\mathbf{V}^{\tilde{n}})$ denotes the eigenvector corresponding to the largest eigenvalue of $\mathbf{V}^{\tilde{n}}$.
-

In the \tilde{n} th iteration for a given feasible point, $\mathbf{V}^{\tilde{n}}$, by replacing $\|\mathbf{V}\|$ with its lower bound $\overline{\mathbf{V}}^{\tilde{n}}$, we can find an upper bound on problem (34) by solving the following optimization problem:

$$\min_{p_m, p_s, \mathbf{V}} \|\mathbf{V}\|_* - \overline{\mathbf{V}}^{\tilde{n}} \quad (36a)$$

$$\text{s.t. (26e), (29d) – (29f), (30), (31).} \quad (36b)$$

Note that problem (36) is a convex semidefinite program (SDP), which can be efficiently solved by existing convex optimization solvers such as CVX [33]. The proposed SCA based algorithm for solving problem (34) is summarized in **Algorithm 1**, where the matrix solution obtained in a given iteration is used as the feasible point for the next iteration. By iteratively solving problem (36), the objective function of (36) is monotonically non-increasing and the proposed **Algorithm 1** is guaranteed to converge to a stationary point of (34).

The overall bisection search based algorithm for determining the elements of \mathbf{U}^{NOMA} is summarized in **Algorithm 2**, where **Algorithm 1** is applied to check the feasibility of problem (32) for a given rate target \bar{r}_0^t . Note that in **Algorithm 1**, a feasible matrix \mathbf{V}^0 , which does not have to be rank-one, has to be initialized. To find such a matrix, we first solve problem (32) by applying semidefinite relaxation (SDR) and ignoring the rank-one constraint. The relaxed version of (32) can be efficiently solved by existing convex optimization solvers such as CVX [33]. We note that if the relaxed version of (32) is unsolvable, this means that problem (32) is also infeasible for the rate target \bar{r}_0^t . In this case, we do not have to apply the proposed **Algorithm 1**, and can directly enter the next iteration of the bisection search algorithm by updating the current upper bound of the rate target as \bar{r}_0^t . If the relaxed version of (32) is solvable, we initialize \mathbf{V}^0 in **Algorithm 1** with the optimal solution of the relaxed problem, denoted by \mathbf{V}^* , and check the feasibility of problem (32) based on the result obtained from **Algorithm 1**. Furthermore, according to [34], the complexities of solving the relaxed version of (32) and applying **Algorithm 1** are $\mathcal{O}((N+1)^{4.5})$ and $\mathcal{O}(I(N+1)^{4.5})$, respectively, where I denotes the number of iterations needed for convergence of **Algorithm 1**. Thus, the overall complexity of **Algorithm 2** with two user decoding order options is $\mathcal{O}\left(2\log_2\left(\frac{r_{\max}-r_{\min}}{\varepsilon_0}\right)\left((I+1)(N+1)^{4.5}\right)\right)$, where r_{\max} and r_{\min}

Algorithm 2 Bisection Search based Algorithm for Determining the Elements of \mathbf{U}^{NOMA}

Given $\{\mathbf{q}_{i,j}^\Delta\}$.

- 1: **for** $k = 1, 2$ **do**
- 2: Initialize r_{\max} , r_{\min} , and the k th decoding order option μ_s, μ_m . Set the defined accuracy ε_0 of the bisection search.
- 3: **while** $r_{\max} - r_{\min} \geq \varepsilon_0$, **do**
- 4: Solve problem (32) without the rank-one constraint for given $\bar{r}_0^t = \frac{r_{\max} + r_{\min}}{2}$.
- 5: **if** the relaxed version of (32) is unsolvable, **then**
- 6: Problem (32) is infeasible, $r_{\max} = \bar{r}_0^t$.
- 7: **else**
- 8: Denote the optimal solution of the relaxed problem by \mathbf{V}^* .
- 9: Solve problem (34) by applying **Algorithm 1** with $\mathbf{V}^0 = \mathbf{V}^*$.
- 10: **if** the converged objective function is zero, **then**
- 11: Problem (32) is feasible, $r_{\min} = \bar{r}_0^t$.
- 12: **else**
- 13: Problem (32) is infeasible, $r_{\max} = \bar{r}_0^t$.
- 14: **end if**
- 15: **end if**
- 16: **end while**
- 17: $\bar{r}_0^{k*} = r_{\min}$.
- 18: **end for**
- 19: $\bar{r}_0^* = \arg \max_{k \in \{1,2\}} (\bar{r}_0^{k*})$.

are the initial upper and lower bounds of the bisection search, respectively, and ε_0 denotes the accuracy of the bisection search.

2) *OMA*: Let matrix $\mathbf{U}^{\text{OMA}} \in \mathbb{R}^{X \times Y}$ denote the communication rate map for OMA. The element in row i and column j of \mathbf{U}^{OMA} can be obtained by solving the following problem:

$$[\mathbf{U}^{\text{OMA}}]_{i,j} = \max_{p_m, p_s, \Theta, \bar{r}_0} \bar{r}_0 \quad (37a)$$

$$\text{s.t. } \bar{R}_m^{\text{OMA}}(\mathbf{q}_{i,j}^\Delta) \geq \bar{r}_0, \quad (37b)$$

$$\bar{R}_s^{\text{OMA}}(\mathbf{q}_{i,j}^\Delta) \geq \bar{r}_s, \quad (37c)$$

$$(26d), (26e). \quad (37d)$$

With the auxiliary variables introduced in the previous subsection, problem (37) can be reformulated as follows:

$$[\mathbf{U}^{\text{OMA}}]_{i,j} = \max_{p_m, p_s, \mathbf{V}, \bar{r}_0} \bar{r}_0 \quad (38a)$$

$$\text{s.t. } \text{Tr}(\tilde{\mathbf{H}}_m \mathbf{V}) + \tau_m(\mathbf{q}_{i,j}^\Delta) \geq \frac{(2^{2\bar{r}_0} - 1) \sigma^2}{2p_m}, \quad (38b)$$

$$\text{Tr}(\tilde{\mathbf{H}}_s \mathbf{V}) + \tau_s \geq \frac{(2^{2\bar{r}_s} - 1) \sigma^2}{2p_s}, \quad (38c)$$

$$(26e), (29e), (29f), (29g). \quad (38d)$$

As can be observed, problem (38) has a similar structure as problem (29) in the previous subsection. Therefore, problem (38) can also be efficiently solved by the proposed bisection search based algorithm in **Algorithm 2** with the complexity of $\mathcal{O}\left(\log_2\left(\frac{r_{\max}-r_{\min}}{\varepsilon_0}\right)\left((I+1)(N+1)^{4.5}\right)\right)$, where now only one decoding order has to be considered since OMA does not employ SIC.

D. Graph Theory based Path Solution

With the obtained communication rate map $\mathbf{U}^Z, Z \in \{\text{NOMA}, \text{OMA}\}$, problem (25) is reformulated as follows:

$$\min_{Q,D} \sum_{d=1}^{D-1} \left\| \mathbf{q}_{i_{d+1},j_{d+1}}^\Delta - \mathbf{q}_{i_d,j_d}^\Delta \right\| \quad (39a)$$

$$\text{s.t. } [\mathbf{U}^Z]_{i_d,j_d} \geq \bar{r}_m, Z \in \{\text{NOMA}, \text{OMA}\}, \quad (39b)$$

$$(13c), (13d). \quad (39c)$$

For given \bar{r}_m , we construct a feasible map based on \mathbf{U}^Z as follows:

$$[\mathbf{\Pi}^Z]_{i,j} = \begin{cases} 1, & \text{if } [\mathbf{U}^Z]_{i,j} \geq \bar{r}_m \\ 0, & \text{otherwise} \end{cases}, i \in \mathcal{X}, j \in \mathcal{Y}. \quad (40)$$

To facilitate the application of graph theory, similar to the single-user case, we construct again an undirected weighted graph $G^Z = (V^Z, E^Z), Z \in \{\text{NOMA}, \text{OMA}\}$. Then, problem (25) can be solved by finding the shortest path from \mathbf{q}_I to \mathbf{q}_F in graph G^Z via the Dijkstra algorithm. The details are omitted here for brevity.

Although we have considered a system with one MRU and one SRU so far in this section, the proposed radio map based path planning method can be easily extended to systems⁸ with one MRU and multiple SRUs, which are indexed by $s_k \in \{s_1, s_2, \dots, s_K\} \triangleq \mathcal{S}$ with $K > 1$. In this case, the communication rate map characterization problem for both NOMA and OMA corresponds to finding the maximum expected communication rate of the MRU for each location, such that the communication rate requirements of the K SRUs are satisfied. For NOMA, the resulting communication rate map characterization problem can also be solved with the proposed **Algorithm 2** by exhaustively searching over all $(K+1)!$ possible NOMA user decoding orders. For OMA, the resulting communication rate map characterization problem can be solved with the proposed **Algorithm 2**, where the communication rate is calculated by allocating orthogonal

⁸For systems with multiple MRUs, the robot path planning problem becomes more challenging since the multiple MRUs have to be carefully coordinated to avoid collisions and the communication rate map of each MRU depends on both its own location and the locations of the other MRUs. Therefore, this scenario is beyond the scope of this paper and constitutes an interesting topic for future work.

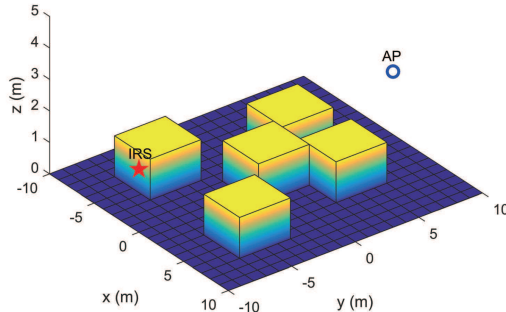


Fig. 4: The simulated scenario (3D view).

frequency bands to the $K + 1$ users. Therefore, the complexity of constructing the communication rate map for NOMA will significantly increase with the number of users due to the required exhaustive search over all possible user decoding orders, while the complexity of OMA does not grow⁹. Based on the communication rate map obtained for NOMA and OMA for systems with one MRU and multiple SRUs, the communication-aware robot path planning problem can be solved by employing graph theory.

IV. NUMERICAL EXAMPLES

In this section, numerical examples are provided to validate the performance of the proposed IRS-enhanced robot navigation system. As illustrated in Fig. 4, we consider an indoor factory (InF) environment with a width \bar{X} and length \bar{Y} of 20 meter, respectively, and a ceiling height of 5 meter. Specifically, the AP and the IRS are deployed at $(0, 10, 2)$ meters and $(0, -10, 2)$ meters, respectively. The number of IRS reflecting elements in each sub-surface is set to $\bar{N} = 20$. The total number of sub-surfaces is $N = N_x N_z$, where N_x and N_z denote the number of sub-surfaces along the x -axis and z -axis, respectively. Therefore, the total number of IRS reflecting elements is $M = \bar{N} N_x N_z$, where we set $N_x = 10$ and increase N_z linearly with M . The considered indoor environment includes 5 obstacles with a size of $4 \times 4 \times 1.3$ m³, respectively. The horizontal centers of the obstacles are located at $(-5, -5)$, $(5, -5)$, $(0, 0)$, $(-3, 4)$, and $(3, 4)$ meters. The height of the antenna of the MRU is $H_0 = 1$ m and its initial and final locations are $\mathbf{q}_I = (-10, 0, 1)$ meters and $\mathbf{q}_F = (10, 0, 1)$ meters, respectively. The path losses of all involved channels are modeled according to the 3rd Generation Partnership Project (3GPP) technical report for the InF-SH (sparse clutter, high BS) scenario [35]. For LoS channels, the path loss in dB is given by

⁹We note that the communication rate map is constructed in an offline manner. Thus, the potentially high complexity of communication rate map computation for NOMA is acceptable given the available computing power.

$$\mathcal{L}_{\text{LoS}} = 31.84 + 21.50 \log_{10}(d) + 19 \log_{10}(f_c), \quad (41)$$

where d denotes the 3D distance between the robotic user and the AP (or the IRS), and $f_c = 2$ GHz is the carrier frequency. For NLoS channels, the path loss in dB is given by

$$\mathcal{L}_{\text{NLoS}} = \max\{\mathcal{L}_{\text{LoS}}, 32.4 + 23 \log_{10}(d) + 20 \log_{10}(f_c)\}, \quad (42)$$

which ensures that $\mathcal{L}_{\text{NLoS}} \geq \mathcal{L}_{\text{LoS}}$. The other system parameters are set as follows: The total transmit power of the AP is $P_{\text{max}} = 20$ dBm, the noise power is $\sigma^2 = -90$ dBm, and the Rician factors of all involved channels are set to 3 dB. To balance between the accuracy of approximating each cell by its center and the computational complexity of robot path planning, we set the threshold for the development of the radio map to $\varepsilon = 0.025$. The corresponding resolutions are $\Delta_x = 0.5 \text{ m} \leq \varepsilon \bar{X}$ and $\Delta_y = 0.5 \text{ m} \leq \varepsilon \bar{Y}$.

A. Single-user Scenario

In this subsection, we demonstrate the effectiveness of the proposed scheme for the single-user scenario. For comparison, we also consider the following benchmark schemes:

- **IRS with discrete phase shifts:** In this case, the IRS is assumed to be equipped with finite resolution phase shifters. We have $\theta_n \in \mathcal{D} = \{0, \delta, \dots, (L-1)\delta\}$, where $\delta = 2\pi/L$ and L denotes the number of discrete phase shift levels. The corresponding channel power gain map is obtained by quantizing the optimal phase shift $\theta_n^*(\mathbf{q}_{i,j}^\Delta)$ in (11) to the nearest discrete phase shift in \mathcal{D} as follows:

$$\theta_n^{\mathcal{D}}(\mathbf{q}_{i,j}^\Delta) = \arg \min_{\theta \in \mathcal{D}} |\theta - \theta_n^*(\mathbf{q}_{i,j}^\Delta)|, \forall n \in \mathcal{N}. \quad (43)$$

- **Without IRS:** In this case, the AP serves the user without the help of an IRS. The channel power gain map is obtained by considering only the AP-user channel.

1) *Channel Power Gain Map:* Fig. 5 illustrates the channel power gain map obtained from (9) with and without IRS, respectively. We set the number of reflecting elements to $M = 1200$. As the MRU cannot enter the regions covered by obstacles, the corresponding expected channel

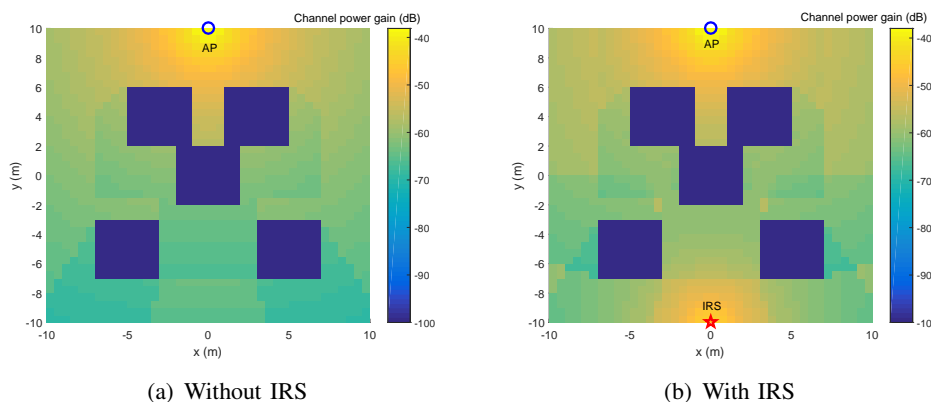


Fig. 5: Illustration of the obtained channel power gain map for different schemes and $\Delta_x = \Delta_y = 0.5 \text{ m}$.

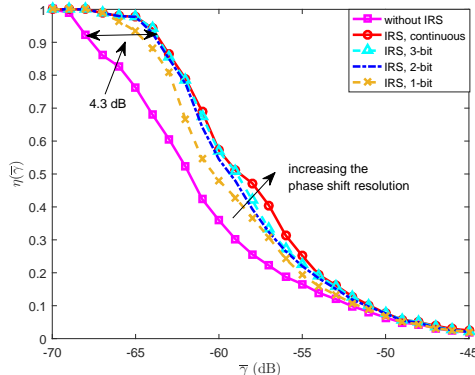


Fig. 6: $\eta(\bar{\gamma})$ versus $\bar{\gamma}$ for different schemes.

power gain is set to $-\infty$. One can observe that the distribution of the channel power gain changes abruptly due to the obstacles. Specifically, as depicted in Fig. 5(a), without IRS, the channel power gains severely degrade if the AP-user link is blocked by obstacles. Moreover, from Fig. 5(b), it can be observed that the channel power gains can be considerably improved by deploying an IRS, especially for the cells around the IRS. The IRS can be interpreted as a virtual AP, however, it is more energy-efficient than an actual AP since the IRS only passively reflects the incident signals.

Based on the obtained channel power gain map, we investigate the percentage of cells, $\eta(\bar{\gamma})$, that can meet the expected channel power gain target, $\bar{\gamma}$. For a given $\bar{\gamma}$, $\eta(\bar{\gamma})$ is calculated as

$$\eta(\bar{\gamma}) = \frac{\sum_{i=1}^X \sum_{j=1}^Y [\mathbf{\Pi}]_{i,j}}{XY - \Upsilon}, \quad (44)$$

where Υ denotes the number of cells which are covered by obstacles. It is observed from Fig. 6 that $\eta(\bar{\gamma})$ decreases for both schemes as the expected channel power gain target increases. Specifically, without IRS, $\eta(\bar{\gamma})$ degrades more quickly than when the IRS is present. The proposed scheme with continuous phase shifts outperforms the scheme without IRS by up to 4.3 dB, which demonstrates the effectiveness of deploying IRSs to reduce the signal dead zones for indoor robotic communication. Moreover, for discrete phase shifts, 1-bit quantization leads to the worst performance as expected since only two phase shifts can be configured, which causes substantial performance loss. The performance achieved by discrete phase shifts approaches the upper bound achieved by continuous phase shifts as the phase shift resolution increases. For 2-bit and 3-bit quantization, the performance gap with respect to the continuous phase shift becomes negligible for most of the expected channel power gain targets, which suggests that 2- or 3-bit phase shifters are promising candidates for practical implementation.

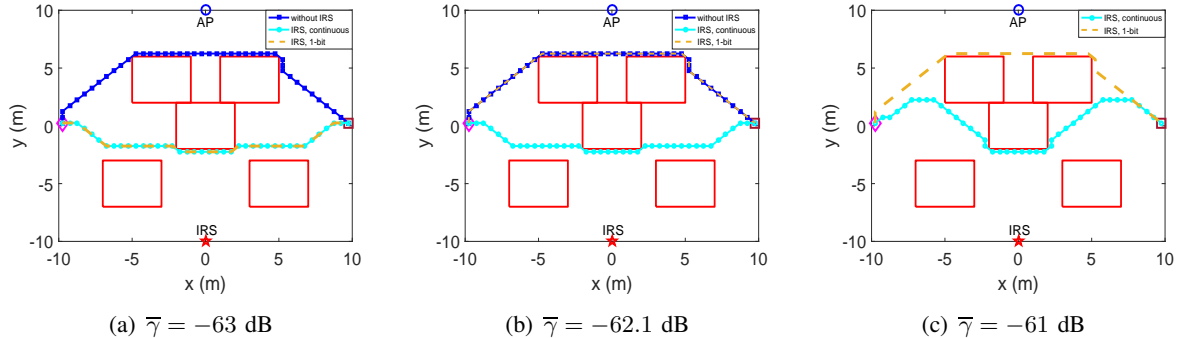


Fig. 7: The obtained path solutions of the MRU for different $\bar{\gamma}$ and $M = 1200$.

2) *Obtained Paths of the MRU*: Fig. 7 depicts the obtained paths of the MRU for different expected channel power gain targets. The red boxes represent the regions covered by obstacles. The initial and final locations of the MRU are denoted by “ \diamond ” and “ \square ”, respectively. For comparison, results without IRS and for 1-bit quantization are also shown. As can be observed in Fig. 7(a), for $\bar{\gamma} = -63$ dB, the path obtained for the case without IRS approaches the AP to avoid the blockage caused by the obstacles. This is expected since only travelling along such a path can create a good channel condition for the MRU, which in turn leads to a longer travelling distance. However, for the IRS-aided schemes, the MRU tends to travel in a relatively straight line from \mathbf{q}_I to \mathbf{q}_F , which leads to a shorter travelling distance compared to the case without IRS. Though the communication link between the MRU and the AP may be blocked by obstacles, a reflected LoS dominated communication link can be established with the IRS. Therefore, the MRU is not forced to travel towards the AP, since the IRS offers more degrees of freedom for path planning. This clearly demonstrates the benefits of deploying an IRS.

In Fig. 7(b), we increase $\bar{\gamma}$ to -62.1 dB. In this case, the path obtained for 1-bit quantization becomes identical to that without IRS. However, the path obtained with the IRS with continuous phase shifts still remains the same as in Fig. 7(a). This is because the performance degradation caused by discrete phase shifts causes some cells to become infeasible even if they are covered by the IRS. As a result, the path planning has to mainly rely on the AP. In Fig. 7(c), the expected channel power gain target is increased further to $\bar{\gamma} = -61$ dB. In this case, the path planning problem becomes infeasible without IRS. For 1-bit quantization, the MRU still needs to travel the longer distance around the AP to meet the expected channel power gain requirement. For the IRS with continuous phase shifts, the MRU tends to travel to regions, which are covered by the IRS through a LoS dominated communication link.

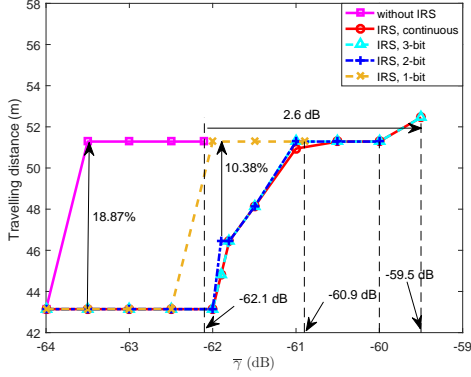


Fig. 8: Travelling distance versus $\bar{\gamma}$ for $M = 1200$.

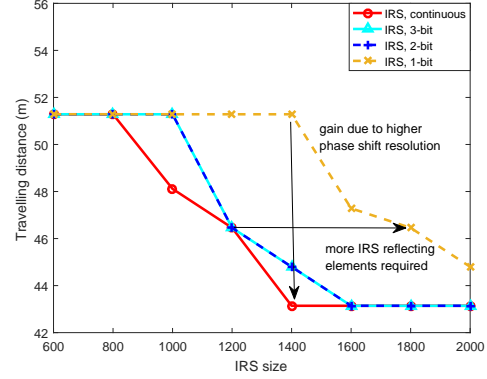


Fig. 9: Travelling distance versus M for $\bar{\gamma} = -61.8$ dB.

3) *Travelling Distance versus Expected Channel Power Gain Target:* In Fig. 8, we depict the travelling distance of different schemes versus the expected channel power gain target $\bar{\gamma}$ for $M = 1200$. It is first observed that the minimum required travelling distances of all schemes generally increase as $\bar{\gamma}$ increases. This is expected since a larger expected channel power gain requirement reduces the number of feasible cells in the radio map, which also reduces the flexibility in path planning. Note that without IRS, the path planning problem becomes infeasible for $\bar{\gamma} \geq -62.1$ dB. The feasibility threshold for the IRS-aided schemes increases to -62.1 dB, -60.9 dB, -60 dB, and -59.5 dB as the phase shift resolution improves. The proposed scheme with continuous phase shifts yields a 2.6 dB performance gain over the scheme without IRS. Moreover, without IRS, when -63.5 dB $\leq \bar{\gamma} \leq -62.5$ dB the MRU needs to travel up to 18.87% farther than when the IRS is present. Furthermore, with the 1-bit phase shifter, the required travelling distance is at most 10.38% larger than for higher phase shift resolutions when -61.9 dB $\leq \bar{\gamma} \leq -60.9$ dB. The performance degradation caused by 2- or 3-bit phase shifters is negligible compared to continuous phase shifters, which is also consistent with the results in Fig. 6.

4) *Travelling Distance versus Number of IRS Elements:* In Fig. 9, the required travelling distance for different schemes versus the number of IRS elements M is presented. We set the expected channel power gain target to $\bar{\gamma} = -61.8$ dB. As can be observed, in general, the minimum required travelling distance of each scheme decreases as M increases. This is because a larger number of IRS elements is capable of achieving a higher array gain, which allows the MRU to travel in a more flexible manner. Furthermore, to achieve the same travelling distance, the 1-bit phase shifter requires at most 600 additional IRS elements compared to the other phase

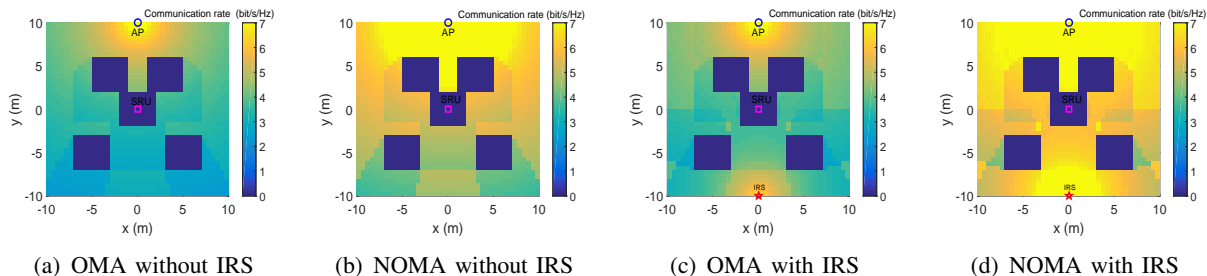


Fig. 10: Illustration of the obtained communication rate map for different schemes and $\Delta_x = \Delta_y = 0.5$ m.

shifters. The performance achieved by 2- or 3-bit phase shifters is close to that for continuous phase shifters. This reveals an interesting trade-off between the number of IRS elements and the number of phase shift resolution bits. Though a smaller number of phase shift resolution bits reduces the cost of the IRS elements, it increases the required number of IRS elements to achieve a certain performance, which in turn increases the deployment cost.

B. Multiple-user Scenario

In this subsection, we consider the multiple-user scenario. Considering the setup in Fig. 4, the SRU's antenna is located at $(0, 0, 1.3)$ meters, such that a LoS dominated communication link to the AP and the IRS always exists. The minimum required communication rate of the SRU is set as $\bar{r}_s = 1$ bit/s/Hz. For comparison, we consider the following benchmark scheme:

- **“Z” without IRS:** In this case, the AP serves multiple users without the help of an IRS. The communication rate map is obtained by solving problems (26) or (37) while only considering the AP-user channels. Here, “Z” refers to NOMA or OMA.

1) *Communication Rate Map:* Fig. 10 depicts the obtained communication rate map for different schemes and $M = 1200$. The location of the SRU is denoted by “□”. As shown in Fig. 10(a), with OMA, only a small region can achieve a rate of more than 5 bit/s/Hz for the MRU, if an IRS is not present. However, in Fig. 10(b), it can be observed that more than half of the cells can achieve a rate of more than 5 bit/s/Hz if NOMA is employed even without the help of an IRS. This is because NOMA allows the two users to share their resource blocks, which improves spectrum efficiency. A significant rate degradation can still be observed in the regions behind the obstacles for both multiple access schemes due to blockage. Fig. 10(c) and Fig. 10(d) show that deploying an IRS significantly improves the expected communication rate, especially for the cells around the IRS. The rate improvement introduced by the IRS is more pronounced for NOMA compared to OMA. In fact, with NOMA, the MRU can achieve a rate of 5 bit/s/Hz or more in 90% of the cells. The rate loss caused by blockages is reduced in the IRS-aided

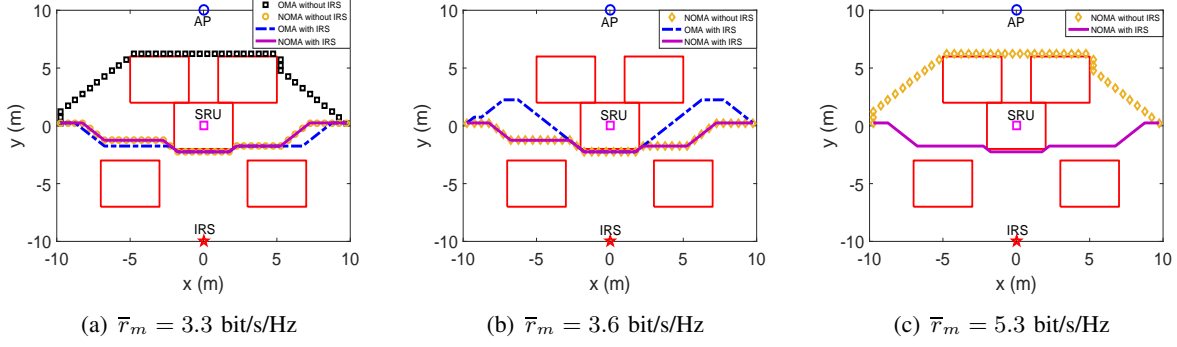


Fig. 11: Paths of MRU for different schemes for given \bar{r}_m and $M = 1200$.

systems since an additional reflected LoS dominated communication link can be established via the IRS.

2) *Obtained Path of the MRU*: Based on the constructed communication rate map, we plot in Fig. 11 the obtained paths for the MRU for different schemes. As shown in Fig. 11(a), when $\bar{r}_m = 3.3$ bit/s/Hz, the MRU needs to take the longer path around the AP only for OMA without IRS, while it takes a more direct path from \mathbf{q}_I to \mathbf{q}_F for the other three schemes. This demonstrates the benefits of NOMA and deploying an IRS. In Fig. 11(b), we increase the required rate from $\bar{r}_m = 3.3$ bit/s/Hz to $\bar{r}_m = 3.6$ bit/s/Hz. In this case, the path planning problem becomes infeasible for OMA without IRS. For NOMA with and without IRS, the path of the MRU remains unchanged, while the path for OMA with IRS tends to traverse the cells covered by the IRS exploiting the reflected LoS dominated channel. In Fig. 11(c), where $\bar{r}_m = 5.3$ bit/s/Hz, the path planning problem becomes infeasible if OMA is used. For NOMA without IRS, the MRU has to approach the AP to achieve the required communication rate, which increases the travelling distance. For NOMA with IRS, the path remains unchanged compared to Fig. 11(b). This underscores the effectiveness of the proposed IRS-aided NOMA scheme.

3) *Travelling Distance versus Required Communication Rate Target*: In Fig. 12, we show the travelling distance versus the required rate target \bar{r}_m for $M = 1200$. We first observe that the travelling distance increases as the required rate target \bar{r}_m increases. Without IRS, the path planning problem becomes infeasible when $\bar{r}_m \geq 3.45$ bit/s/Hz for OMA and $\bar{r}_m \geq 5.3$ bit/s/Hz for NOMA. With IRS, the threshold increases to 3.9 bit/s/Hz for OMA and 6.25 bit/s/Hz for NOMA. With IRS, the gain of NOMA over OMA is more pronounced than without IRS. This is because properly configured the IRS phase shifts can enhance the channel disparity between the two users, which benefits NOMA. Furthermore, it is also observed that for NOMA the IRS gain is more pronounced than for OMA. This implies that deploying an IRS is more beneficial

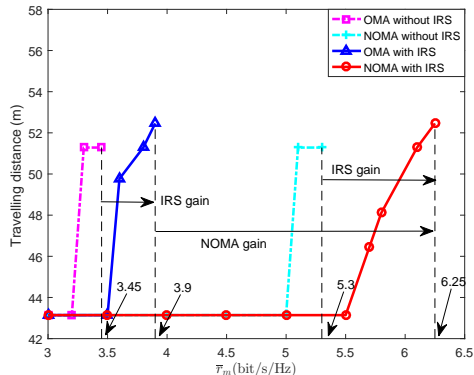


Fig. 12: Travelling distance versus \bar{r}_m for $M = 1200$.

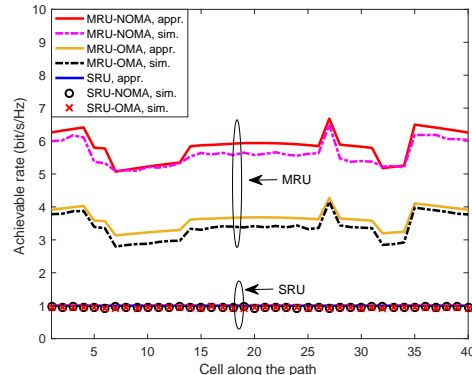


Fig. 13: Comparison of approximate and the exact expected achievable rate.

if NOMA is employed.

4) *Tightness of Expected Achievable Rate Approximation:* In Fig. 13, we evaluate the tightness of the approximation of the expected achievable rate. Specifically, the MRU is assumed to travel along the path in Fig. 11(a) for OMA and NOMA. For each cell along the path, the approximation of the expected achievable rates, i.e., $\bar{R}_l^{\text{NOMA}}(\mathbf{q}_{i,j}^\Delta)$ and $\bar{R}_l^{\text{OMA}}(\mathbf{q}_{i,j}^\Delta)$, are calculated with (22) and (24). The exact expected achievable rates, i.e., $\mathbb{E}[R_l^{\text{NOMA}}(\mathbf{q}_{i,j}^\Delta)]$ and $\mathbb{E}[R_l^{\text{OMA}}(\mathbf{q}_{i,j}^\Delta)]$, are obtained via Monte Carlo simulation by averaging over 10000 random channel realizations for each cell. As can be observed, the approximations match well with the exact results for the SRU for OMA and NOMA. For the MRU, a small gap can be observed between the approximation and the exact results since the approximation is an upper bound for the exact average achievable rate. This implies that, in a practical implementation, a small constant should be added to the required rate \bar{r}_m in the proposed optimization problem (25) to account for the gap between the upper bound and the actual average achievable rate.

V. CONCLUSIONS

An IRS-assisted indoor robot navigation system has been investigated. The communication-aware robot path planning problem was formulated for minimization of the travelling time/distance by jointly optimizing the robot path and the phase shifts of the IRS elements. To solve this problem, we proposed a radio map based approach which exploits knowledge about the location-dependent channel propagation. Channel power gain maps and the communication rate maps were constructed for single-user and multiple-user systems, respectively. Based on these two radio maps, the robot path planning problem was efficiently solved by invoking graph theory. Numerical results showed that the coverage of the AP can be significantly extended by deploying

an IRS, and the robot travelling distance can be significantly reduced with the aid of an IRS and NOMA.

This paper assumed perfect knowledge of the geographic information of the considered indoor environments, which can be difficult to obtain in some applications (e.g., search and rescue missions). An important direction for future research is to investigate communication-aware robot path planning in uncertain environments. In this case, simultaneous localization and mapping (SLAM) [36] may be a promising approach to assist radio map construction.

APPENDIX A: PROOF OF LEMMA 1

The expected effective channel power gain of the MRU, $\mathbb{E} [|c_m(t)|^2]$, can be decomposed as follows:

$$\begin{aligned} \mathbb{E} [|c_m(t)|^2] &= \mathbb{E} \left\{ \left| \left(\tilde{h}_m^H(\mathbf{q}(t)) + \check{h}_m^H \right) + \left(\tilde{\mathbf{r}}_m^H(\mathbf{q}(t)) + \check{\mathbf{r}}_m^H \right) \Theta(t) (\tilde{\mathbf{g}} + \check{\mathbf{g}}) \right|^2 \right\} \\ &\stackrel{(a)}{=} |x_1|^2 + \mathbb{E} \{|x_2|^2\} + \mathbb{E} \{|x_3|^2\} + \mathbb{E} \{|x_4|^2\} + \mathbb{E} \{|x_5|^2\}, \end{aligned} \quad (45)$$

where $\tilde{h}_m^H(\mathbf{q}(t)) = \sqrt{\frac{\mathcal{L}_{AM}(\mathbf{q}(t))K_{AM}(\mathbf{q}(t))}{K_{AM}(\mathbf{q}(t))+1}} \tilde{h}_m^H(\mathbf{q}(t))$, $\check{h}_m^H = \sqrt{\frac{\mathcal{L}_{AM}(\mathbf{q}(t))}{K_{AM}(\mathbf{q}(t))+1}} \hat{h}_m^H$, $\tilde{\mathbf{r}}_m^H(\mathbf{q}(t)) = \sqrt{\frac{\mathcal{L}_{IM}(\mathbf{q}(t))K_{IM}(\mathbf{q}(t))}{K_{IM}(\mathbf{q}(t))+1}} \tilde{\mathbf{r}}_m^H(\mathbf{q}(t))$, $\check{\mathbf{r}}_m^H = \sqrt{\frac{\mathcal{L}_{IM}(\mathbf{q}(t))}{K_{IM}(\mathbf{q}(t))+1}} \hat{\mathbf{r}}_m^H$, $\tilde{\mathbf{g}} = \sqrt{\frac{\mathcal{L}_{AI}K_{AI}}{K_{AI}+1}} \hat{\mathbf{g}}$, and $\check{\mathbf{g}} = \sqrt{\frac{\mathcal{L}_{AI}}{K_{AI}+1}} \hat{\mathbf{g}}$. In (45), (a) is due to the fact that \tilde{h}_m^H , \check{h}_m^H , and $\check{\mathbf{g}}$ have zero means and are independent from each other. We have

$$|x_1|^2 = \left| \tilde{h}_m^H(\mathbf{q}(t)) + \tilde{\mathbf{r}}_m^H(\mathbf{q}(t)) \Theta(t) \tilde{\mathbf{g}} \right|^2, \quad (46a)$$

$$\mathbb{E} \{|x_2|^2\} = \mathbb{E} \left\{ \left| \check{h}_m^H \right|^2 \right\} = \frac{\mathcal{L}_{AM}(\mathbf{q}(t))}{K_{AM}(\mathbf{q}(t)) + 1}, \quad (46b)$$

$$\mathbb{E} \{|x_3|^2\} = \mathbb{E} \left\{ \left| \tilde{\mathbf{r}}_m^H(\mathbf{q}(t)) \Theta(t) \check{\mathbf{g}} \right|^2 \right\} = \frac{\mathcal{L}_{AI} \mathcal{L}_{IM}(\mathbf{q}(t)) K_{IM}(\mathbf{q}(t)) M}{(K_{AI} + 1)(K_{IM}(\mathbf{q}(t)) + 1)}, \quad (46c)$$

$$\mathbb{E} \{|x_4|^2\} = \mathbb{E} \left\{ \left| \check{\mathbf{r}}_m^H(\mathbf{q}(t)) \Theta(t) \tilde{\mathbf{g}} \right|^2 \right\} = \frac{\mathcal{L}_{AI} K_{AI} \mathcal{L}_{IM}(\mathbf{q}(t)) M}{(K_{AI} + 1)(K_{IM}(\mathbf{q}(t)) + 1)}, \quad (46d)$$

$$\mathbb{E} \{|x_5|^2\} = \mathbb{E} \left\{ \left| \check{\mathbf{r}}_m^H(\mathbf{q}(t)) \Theta(t) \check{\mathbf{g}} \right|^2 \right\} = \frac{\mathcal{L}_{AI} \mathcal{L}_{IM}(\mathbf{q}(t)) M}{(K_{AI} + 1)(K_{IM}(\mathbf{q}(t)) + 1)}. \quad (46e)$$

Therefore, by inserting the results in (46a)-(46e) into (45), we arrive at (5). This completes the proof of Lemma 1.

REFERENCES

- [1] X. Mu, Y. Liu, L. Guo, J. Lin, and R. Schober, "Intelligent reflecting surface enhanced indoor robot path planning using radio maps," in *Proc. IEEE Int. Conf. Commun. (ICC)*, 2021, [Online]. Available: <https://arxiv.org/abs/2009.11519>.
- [2] B. Siciliano and O. Khatib, *Springer Handbook of Robotics*. Springer, 2008.
- [3] G. Hu, W. P. Tay, and Y. Wen, "Cloud robotics: architecture, challenges and applications," *IEEE Network*, vol. 26, no. 3, pp. 21–28, 2012.
- [4] M. Dunbabin and L. Marques, "Robots for environmental monitoring: Significant advancements and applications," *IEEE Robotics Automation Magazine*, vol. 19, no. 1, pp. 24–39, 2012.
- [5] P. Galambos, "Cloud, fog, and mist computing: Advanced robot applications," *IEEE Systems, Man, and Cybernetics Magazine*, vol. 6, no. 1, pp. 41–45, 2020.

- [6] Q. Wu and R. Zhang, "Towards smart and reconfigurable environment: Intelligent reflecting surface aided wireless network," *IEEE Commun. Mag.*, vol. 58, no. 1, pp. 106–112, 2020.
- [7] Y. Liu, X. Liu, X. Mu, T. Hou, J. Xu, Z. Qin, M. D. Renzo, and N. Al-Dhahir, "Reconfigurable intelligent surfaces: Principles and opportunities," [Online]. Available: <https://arxiv.org/abs/2007.03435>.
- [8] M. D. Renzo, A. Zappone, M. Debbah, M. Alouini, C. Yuen, J. D. Rosny, and S. Tretyakov, "Smart radio environments empowered by reconfigurable intelligent surfaces: How it works, state of research, and road ahead," *IEEE J. Sel. Areas Commun.*, vol. 38, no. 11, pp. 2450–2525, 2020.
- [9] Y. Liang, R. Long, Q. Zhang, J. Chen, H. V. Cheng, and H. Guo, "Large intelligent surface/antennas (LISA): Making reflective radios smart," *J. Commun. Inf. Networks*, vol. 4, no. 2, pp. 40–50, 2019.
- [10] C. Huang, S. Hu, G. C. Alexandropoulos, A. Zappone, C. Yuen, R. Zhang, M. Di Renzo, and M. Debbah, "Holographic MIMO surfaces for 6G wireless networks: Opportunities, challenges, and trends," *IEEE Wireless Commun.*, vol. 27, no. 5, pp. 118–125, 2020.
- [11] R. Robotin, G. Lazea, and C. Marcu, *Graph Search Techniques for Mobile Robot Path Planning*. INTECH, 2010.
- [12] Y. Zhang, D.-W. Gong, and J.-H. Zhang, "Robot path planning in uncertain environment using multi-objective particle swarm optimization," *Neurocomputing*, vol. 103, pp. 172–185, 2013.
- [13] P. Bhattacharjee, P. Rakshit, I. Goswami, A. Konar, and A. K. Nagar, "Multi-robot path-planning using artificial bee colony optimization algorithm," in *3rd World Congr. on Nature and Biologically Inspired Comput. (NaBIC)*, 2011, pp. 219–224.
- [14] B. Sangiovanni, G. P. Incremona, M. Piastra, and A. Ferrara, "Self-configuring robot path planning with obstacle avoidance via deep reinforcement learning," *IEEE Control Syst. Lett.*, vol. 5, no. 2, pp. 397–402, 2021.
- [15] Q. Wu and R. Zhang, "Intelligent reflecting surface enhanced wireless network via joint active and passive beamforming," *IEEE Trans. Wireless Commun.*, vol. 18, no. 11, pp. 5394–5409, 2019.
- [16] C. Huang, A. Zappone, G. C. Alexandropoulos, M. Debbah, and C. Yuen, "Reconfigurable intelligent surfaces for energy efficiency in wireless communication," *IEEE Trans. Wireless Commun.*, vol. 18, no. 8, pp. 4157–4170, 2019.
- [17] X. Yu, D. Xu, Y. Sun, D. W. K. Ng, and R. Schober, "Robust and secure wireless communications via intelligent reflecting surfaces," *IEEE J. Sel. Areas Commun.*, vol. 38, no. 11, pp. 2637–2652, 2020.
- [18] C. Huang, G. C. Alexandropoulos, C. Yuen, and M. Debbah, "Indoor signal focusing with deep learning designed reconfigurable intelligent surfaces," in *Proc. IEEE 20th Int. Workshop Signal Process. Adv. Wireless Commun. (SPAWC)*, 2019, pp. 1–5.
- [19] C. Pan, H. Ren, K. Wang, W. Xu, M. ElKashlan, A. Nallanathan, and L. Hanzo, "Multicell MIMO communications relying on intelligent reflecting surfaces," *IEEE Trans. Wireless Commun.*, vol. 19, no. 8, pp. 5218–5233, 2020.
- [20] C. Huang, R. Mo, and C. Yuen, "Reconfigurable intelligent surface assisted multiuser MISO systems exploiting deep reinforcement learning," *IEEE J. Sel. Areas Commun.*, vol. 38, no. 8, pp. 1839–1850, 2020.
- [21] S. Li, B. Duo, X. Yuan, Y. Liang, and M. Di Renzo, "Reconfigurable intelligent surface assisted UAV communication: Joint trajectory design and passive beamforming," *IEEE Wireless Commun. Lett.*, vol. 9, no. 5, pp. 716–720, 2020.
- [22] T. Hou, Y. Liu, Z. Song, X. Sun, Y. Chen, and L. Hanzo, "Reconfigurable intelligent surface aided NOMA networks," *IEEE J. Sel. Areas Commun.*, vol. 38, no. 11, pp. 2575–2588, 2020.
- [23] X. Mu, Y. Liu, L. Guo, J. Lin, and N. Al-Dhahir, "Exploiting intelligent reflecting surfaces in NOMA networks: Joint beamforming optimization," *IEEE Trans. Wireless Commun.*, vol. 19, no. 10, pp. 6884–6898, 2020.
- [24] S. Bi, J. Lyu, Z. Ding, and R. Zhang, "Engineering radio maps for wireless resource management," *IEEE Wireless Commun.*, vol. 26, no. 2, pp. 133–141, 2019.
- [25] M. Najafi, V. Jamali, R. Schober, and H. Vincent Poor, "Physics-based modeling and scalable optimization of large intelligent reflecting surfaces," *IEEE Trans. Commun.*, Early Access, 2020, doi: 10.1109/TCOMM.2020.3047098.
- [26] Y. Yang, B. Zheng, S. Zhang, and R. Zhang, "Intelligent reflecting surface meets OFDM: Protocol design and rate maximization," *IEEE Trans. Commun.*, vol. 68, no. 7, pp. 4522–4535, 2020.
- [27] B. Zheng and R. Zhang, "Intelligent reflecting surface-enhanced OFDM: Channel estimation and reflection optimization," *IEEE Wireless Commun. Lett.*, vol. 9, no. 4, pp. 518–522, 2020.
- [28] X. Mestre, "Improved estimation of eigenvalues and eigenvectors of covariance matrices using their sample estimates," *IEEE Trans. Inf. Theory*, vol. 54, no. 11, pp. 5113–5129, 2008.
- [29] K. Werner, M. Jansson, and P. Stoica, "On estimation of covariance matrices with Kronecker product structure," *IEEE Trans. Signal Process.*, vol. 56, no. 2, pp. 478–491, 2008.
- [30] D. B. West, *Introduction to Graph Theory*. Englewood Cliffs, NJ: Prentice-Hall, 1996.
- [31] Y. Liu, Z. Qin, M. ElKashlan, Z. Ding, A. Nallanathan, and L. Hanzo, "Nonorthogonal multiple access for 5G and beyond," *Proc. IEEE*, vol. 105, no. 12, pp. 2347–2381, 2017.
- [32] Q. T. Dinh and M. Diehl, "Local convergence of sequential convex programming for nonconvex optimization," *Recent Advances in Optimization and its Applications in Engineering*, Springer, 2010.
- [33] M. Grant and S. Boyd, "CVX: Matlab software for disciplined convex programming, version 2.1," [Online]. Available: <http://cvxr.com/cvx>, 2014.
- [34] Z. Luo, W. Ma, A. M. So, Y. Ye, and S. Zhang, "Semidefinite relaxation of quadratic optimization problems," *IEEE Signal Process. Mag.*, vol. 27, no. 3, pp. 20–34, 2010.
- [35] 3GPP-TR-38.901, "Study on channel model for frequencies from 0.5 to 100 GHz," 2017, 3GPP technical report. [Online]. Available: www.3gpp.org/DynaReport/38901.htm.

- [36] M. W. M. G. Dissanayake, P. Newman, S. Clark, H. F. Durrant-Whyte, and M. Csorba, "A solution to the simultaneous localization and map building (SLAM) problem," *IEEE Trans. Robot. Automat.*, vol. 17, no. 3, pp. 229–241, 2001.